3-22-2023

Super–protonic conductors for solid acid fuel cells (SAFCs): a review

Sh. Afroze
L.N. Gumilyov Eurasian National University;Faculty of Integrated Technologies, Universiti Brunei Darussalam ,Kazakhstan

Md S. Reza
L.N. Gumilyov Eurasian National University;Faculty of Integrated Technologies, Universiti Brunei Darussalam ,Kazakhstan

M.R. Somalu
Fuel Cell Institute, Universiti Kebangsaan Malaysia ,Malaysia

A.K. Azad
Faculty of Integrated Technologies, Universiti Brunei Darussalam ,Brunei Darussalam ,

Follow this and additional works at: https://www.ephys.kz/journal

Part of the Materials Science and Engineering Commons, and the Physics Commons

Recommended Citation

Super–protonic conductors for solid acid fuel cells (SAFCs): a review

Sh. Afroze[*,1,2], Md S. Reza[1,2],
M.R. Somalu[3], A.K. Azad[*,2]

[1]L.N. Gumilyov Eurasian National University, Astana, Kazakhstan

[2]Faculty of Integrated Technologies, Universiti Brunei Darussalam, Bandar Seri Begawan, Brunei

[3]Fuel Cell Institute, Universiti Kebangsaan Malaysia, Selangor, Malaysia

E-mail: shammya111@gmail.com; abul.azad@ubd.edu.bn

Fuel cell holds the promise of being environmentally friendly and becomes one of the alternatives for renewable energy. Solid acids have super–protonic behavior which allows them to become conductors. It can function at high temperatures. Hydration, on the other hand, may be used to improve the performance of the solid acid. Moreover, the conductivity, stability, and crystal structure of the solid acid compounds of the fuel cell are all influenced by the size of the electrolyte membrane. Very few works have been done on solid acid fuel cells which are still under investigation to make it one viable as well as a reliable alternative to clean, renewable energy. In general, this work will provide an overview of the variables or characteristics that affect the technical effectiveness and performance of the unique super–protonic conductors for solid acid fuel cells.

Keywords: fuel cells; solid acid fuel cells (SAFCs); super protonic conductors; electrolytes; renewable energy

Nomenclature

O_2	Oxygen
H_2	Hydrogen
H_2O	Water
H_2SO_4	Sulphuric acid
$CsHSO_4$	Caesium hydrogen sulphate
AFC	Alkaline fuel cell
CDP	$CsHSO_4$ – caesium hydrogen sulphate
DMFC	Direct methanol fuel cell
DTA	Differential Thermal Analysis
GHG	Greenhouse gas
HPA	Hetaopolyacid
MCFC	Molten carbonate fuel cell
PAFC	Phosphoric acid fuel cell
PEMC	Proton exchange membrane fuel cells
SAFC	Solid acid fuel cell
SOFC	Solid oxide fuel cell

Introduction

Due to rising urbanization and industrialization, population increase constitutes a significant worldwide problem for energy, resource management, and development [1, 2]. The main and primary demand in the present society is an uninterrupted power supply which can come from various sources like coal, petroleum, nuclear, solar, and wind [3, 4]. Conventional fossil fuels will power this substantial human population for another 50 years [5, 6]. However, to meet this enormous energy demand, fossil fuels have reached the brink of extinction and emit harmful gases, especially greenhouse gas (GHG) [7–12]. Global greenhouse gas (GHG) emissions must, however, decline by 50% by 2030 and reach net zero by the middle of the century if the worst effects of climate change are to be avoided [13]. Therefore, it is imperative to develop more effective technologies to avoid these toxic gases [14–17]. Our usage of clean technologies must expand by at least one order of magnitude if we are to decarbonize our energy supply and achieve its net zero goals [18].

The challenges of reducing greenhouse gas emissions from the usage of fossil fuels and diversifying renewable sources depend on energy conversion and storage [19–21]. By increasing the percentage of renewable energy sources used in energy generation, significant progress has been made in decreasing emissions. The intermittent nature of renewable energy sources has drawn attention to energy conversion and storage, which has in turn sparked intense interest in the generation of carbon–free energy [22, 23]. Systems for energy conversion and storage that are extremely resilient, retrofittable, and sustainable in order to make the most of the world's strategic component inventories and prevent their depletion [24]. Many research have been conducted on various Li-ion batteries [25–27], supercapacitors [27–29], solid oxide fuel cells (SOFCS) [30–32], solid

acid fuel cells (SAFCs) [33], proton exchange membrane fuel cells (PMFCs) [34], and dye-sensitized solar cells [35–37] for the generation of renewable energy. In electrode and electrolyte developments, the current problems with energy conversion and storage technologies are well–documented. The core problem for these technologies is to find the ideal electrode and electrolyte materials [38–40].

To attain high strength, power density, and system efficiency, functional materials are necessary that combine the chemical qualities needed for increased performance with chemical and electrical stability [41]. It should be required that these environmentally friendly products have little or no impact. With attentive consideration, it can be observed that selecting appropriate electrolyte and electrode materials, the electronic structure, and modeling is essential to triumphing the desired performance [42]. One of the most widely used technologies for converting and storing energy is the fuel cell, which is unquestionably seen as the technology of the future [43, 44]. Fuel cells have received a lot of attention as a potential technology for clean and efficient power production for stationary and mobile applications because of their high efficiency and minimal impact on the environment [45, 46]. Figure 1 displays a comparison graph of several fuel cells at various operating temperatures [47].

In order to convert the chemical energy from the fuel into electrical energy, a fuel cell uses chemical processes to generate electricity [48–51]. In the fuel cell system, an electrolyte connects the positively charged cathode to a negatively charged anode [52–55]. Unlike batteries, the fuel cell does not store energy and does not need the power to charge . Thus fuel cells will generate electricity continuously as long as it has supplied with fuel. It has high efficiencies and low pollutions level because of that, it becomes another alternative for electrical power generation [56].

As the thermodynamic systems for producing electricity evolve, more attention is being devoted to the development of fuel cells, in which oxygen and hydrogen (as a fuel) undergo an electrochemical reaction to produce water and ingest a reactant from an external source [57, 58]. The energy is converted electrochemically as the fuel is not blazed unlike other internal combustion engines [59, 60]. Due to the protection of heat output of the reaction, fuel cells can become two to three times more effective than thermal power plants or internal combustion engines [61].

For the Gemini space missions in the early 1960s, Willard Thomas Grubb and Leonard Niedrach of NASA in the United States were the first to use PEMFCs [62]. Due to its low operating temperature (60–250 $^\circ$ C) [63, 64], it has been used broadly in the alternative energy production sectors. But the PEM fuel cells require platinum cathodes which are costly and more heed is being paid to developing an alternative to PEMFCs. As a consequence, transitional metal oxides which are not platinum alloys have been produced to make solid acid fuel cells [65], cesium hydrogen sulfate, abbreviated $CsHSO_4$, is the name of this solid acid that serves as an electrolyte. $CsHSO_4$ may be utilized in fuel cells without having to be hydrated. Solid acids are salts that resemble acids and have temperature–controlled superprotonic conductivity. Comparing solid acid electrolytes to polymer electrolytes, there are several benefits to be had. Solid
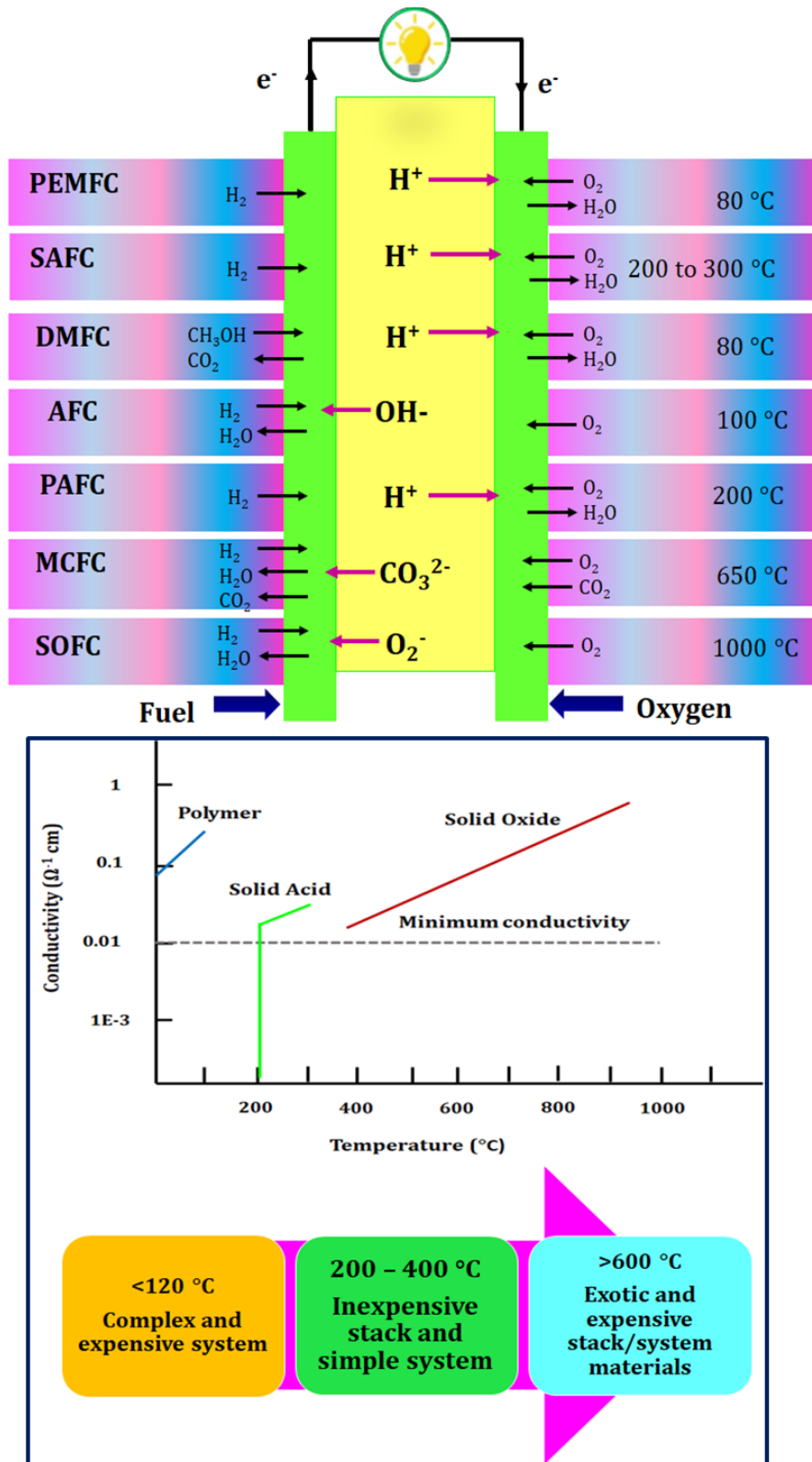
Figure 1. Contrasting the various fuel cell types and their characteristics of fuel cell electrolytes [47].

acid fuel cells, which function anhydrous at a significantly higher temperature, are unaffected by PEMFC problems such as the constant humidification demand and catalyst poisoning caused by low operational temperatures [66]. Thus, when left at room temperature, solid acids show a little protonic conduction. When
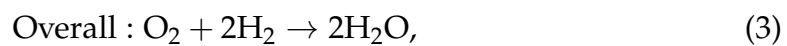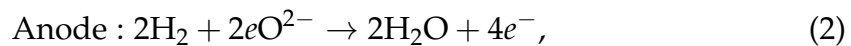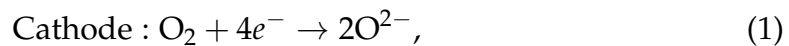
heated, they reach a point where they "all of a sudden" experience a phase shift and have super protonic conductivity.

In order to identify the factors or components that influence the functioning and efficacy of this particular fuel cell type, this study aims to assess the electrolyte behavior in the super–protonic conductors of solid acid fuel cells. In this work, we highlight the proton transport mechanism and the super protonic behavior of solid acids and also focuses on why solid electrolytes are favored to liquid ones in an intermediate temperature range. By comparing it to other types of fuel cells, the advantages and drawbacks of the electrolytes are briefly discussed, along with the characteristics of the substances.

State–of the art of fuel cells

As a source of clean energy, a fuel cell is ecologically benign. This fundamental idea of the fuel cell is drawn from electrochemistry, a subfield of chemistry, which deals with the generation of electricity through chemical reactions [67, 68]. All chemical elements can participate in chemical reactions with each other spontaneously based on their specific conditions. For instance, If different types of materials are mixed with strong acids like sulphuric acid (H_2SO_4), they can react strongly with different substances [69]. With these kinds of fuel cells, the reaction is only set up between hydrogen and oxygen.

When they allow spontaneous movement they release heat energy – and this type of spontaneous reaction is called an exothermic reaction. All the chemical reactions that may be exploited to come up with electrical energy are spontaneous reactions. Then again, when the reaction is affected electrochemically, the advancement of the response is overseen so that a portion of the energy that would regularly be delivered as warmth rises rather than electrical energy. The following describes the reaction that occurs at the anode and cathode:

$$Cathode : O_2 + 4e^- \rightarrow 2O^{2-}, \tag{1}$$

$$Anode : 2H_2 + 2eO^{2-} \rightarrow 2H_2O + 4e^-, \tag{2}$$

$$Overall : O_2 + 2H_2 \rightarrow 2H_2O, \tag{3}$$

The anode is where hydrogen enters the fuel cell. In order to speed the release of oxygen ions from a hydrogen–containing electrolyte, the anode can aid in the adsorption of hydrogen and oxygen along the fuel pathway. The hydrogen molecules lose their electrons in a chemical process, causing the atoms to ionize and produce H^+. To generate current, the electrons move across wires. The oxygen usually comes from the air and enters at the cathode. The oxygen absorbs the electrons once they have finished their circuit. The waste product that leaves the fuel cell is water (H_2O), which is generated when the oxygen reacts with the ionized hydrogen atoms (H^+). Moreover, electrolyte is very crucial. It restricts

which ions may go back and forth between the cathode and anode. A fuel cell, therefore, requires air and hydrogen (H_2) to function (O_2) [70, 71].

As oxygen molecules come into contact with the cathode, they will stick to the electrode surface and become separated, leaving each with two oxygen atoms. Be that as it may, these require the flexibility of electrons in the event that they are to frame oxygen ions [72]. Just in this structure, they would be able to converge with the hydrogen ions going through the electrolyte from the anode to make water molecules. The electrons must originate from the anode, however, these electrons can not go through the electrolyte. On the off chance that an electrical association is made between the two electrodes, the electrons would now be able to go through the interfacing wire to the oxygen atoms, to make oxygen ions, permitting the reaction to race to finishing. The above standard of the fuel cell model was summed up in Figure 2. The electrolyte assumes a significant part in a fuel cell; consequently, they are commonly distinguished by the sort of electrolyte that is executed.
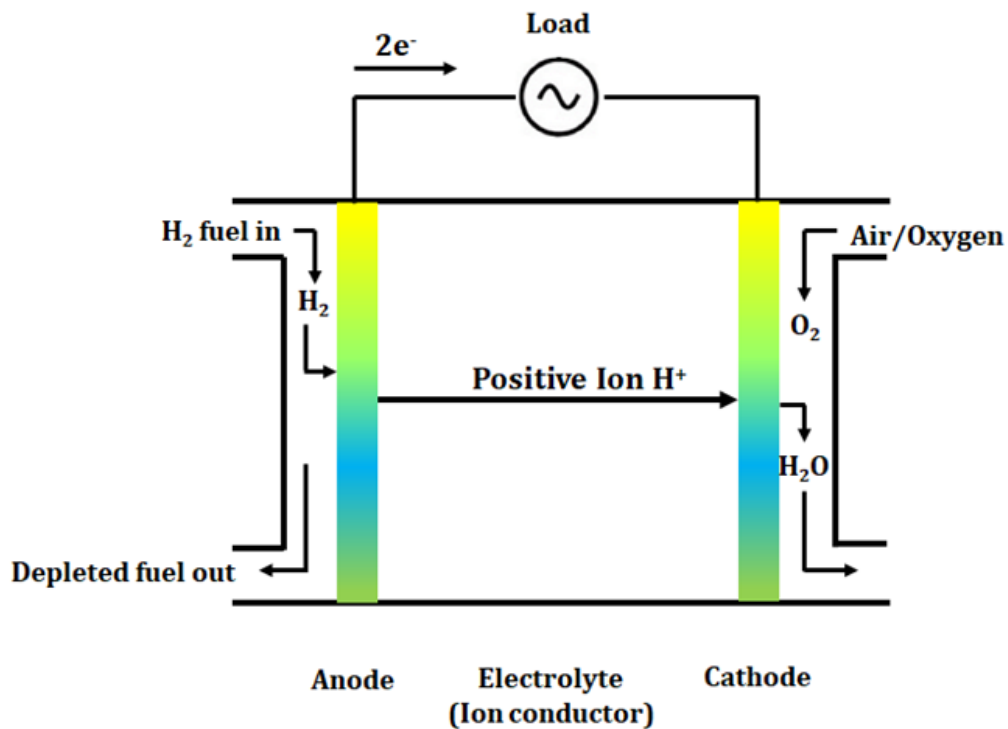

Figure 2. The principle of the hydrogen fuel cell [73].

Nowadays, a variety of fuel cell types are commercially accessible, including molten carbonate fuel cells (MCFCs), proton exchange membrane fuel cells (PEMFCs), direct methanol fuel cells (DMFCs), alkaline fuel cells (AFCs), soild acid fuel cells (SAFCs), solid oxide fuel cells (SOFCs), proton ceramic fuel cells (PCFCs) and phosphoric acid fuel cells (PEMFCs) [74]. As was previously noted in the fuel cell concept, the chemical configuration of the electrolyte in each fuel cell makes them distinct from one another. Different electrolytes have varying efficiencies that change with temperature, allowing each kind to operate in a different temperature range. Table 1 lists several fuel cell types along with their temperature and electrolytes, accordingly.

Table 1.
Types of Fuel Cells [75].

Type of the Fuel cell	Electrolyte	Temperature Range	Fuel
Proton exchange membrane fuel cell (PEMFC)	Sulfonated polymers, e.g., Nafion (Proton conducting membrane)	20–120°C	Hydrogen
Direct methanol fuel cell (DMFC)	Polymer membrane	60–130°C	Methanol
Alkaline fuel cell (AFC)	Aqueous KOH (Caustic potash solution)	100–200°C	Hydrogen
Solid acid fuel cell (SAFC)	Solid acids, e.g. $CsHSO_4$	100–300°C	Propane, methane, methanol, or diesel
Phosphoric acid fuel cell (PAFC)	H_3PO_4 (Concentrated phosphoric acid)	150–200°C	Hydrogen
Molten carbonate fuel cell (MCFC)	$(NA,K)_2CO_3$ (Molten carbonate)	600–700°C	Natural Gas, coal, biogas
Solid oxide fuel cell (SOFC)	$(Zr, Y)O_{2-3}$ (Ceramic)	700–1000°C	Hydrogen, natural gas, biogas, or a mixture with hydrogen

Due to the excellent power density at low operating temperatures, direct alcohol fuel cells (DAFC) and proton–exchange–membrane fuel cells (PEMFC) are frequently utilized in portable electronic technologies [76]. One of the key issues preventing the effective commercialization of DMFC is their high production cost. Also, the significant drawback of PEMFCs is that they raise the cost of the unit as a result of needing a costly catalyst, in this instance platinum [77]. Although CO_2 still has an impact on performance and durability, AFCs are being evaluated for applications in the W to kW range. Because to their working temperatures and lack of materials, MCFC and PAFC still have certain commercialization restrictions. The reduction of the cathodes of molecular oxygen is a significant drawback for the MCFC system [78] and the performance of the oxygen–reducing electrode, or cathode, is the primary drawback of PAFC [77]. Because of its promising advantages, SOFC is still a desirable prospective alternative today, as evidenced by the fact that this technology is being used in more and more applications today, particularly in the sectors of portable power production and transportation [79, 80]. Noteworthy, SOFCs based on proton–conducting electrolytes are also referred to as protonic ceramic fuel cells (PCFCs) [81, 82]. By adopting affordable manufacturing techniques, PCFCs have made it feasible to attain significantly greater cell power densities at lower working temperatures (400–600 °C), potentially resulting in lower stack costs than traditional SOFC

technology [83]. As the materials utilized as components in SOFCs work at high temperatures, hence they face thermal challenges. Overall, solid acid fuel cells (SAFCs) are a natural gas–powered, long–lasting technology that is suitable for applications involving dispersed generation. When compared to centralized power plants, these distributed generating technologies will incur less expense in operational expenses due to peak shaving and lower costs associated with power losses [84]. Because of its low–cost parts, quick and simple installation, fuel flexibility and efficiency, and minimal maintenance requirements, SAFC attracts researchers and consumers in commercialization every day.

Advantages and drawbacks of fuel cells

There are various benefits to fuel cell technology, as follows [85, 86]:

- Having the possibility for high operating effectiveness;

- Fuel availability and various methods of supplying fuel to the fuel cell;

- Having an exceptionally versatile design;

- Unlike natural gases and coals, do not release any carbon dioxide or other greenhouse gases that cause global warming, lowering pollution and enhancing air quality;

- Low in maintenance since they do not have any moving parts;

- There is no recharge required, and they provide power instantly as the fuel is supplied to the fuel cell.

Despite the advantages of the fuel cell, there are also drawbacks of it as the following:

- Costly because of the requirement for materials with explicit properties. This incorporates the interest in platinum and Nafion materials;

- Reformation of the innovation can be expensive and cumbersome and needs the capacity to run;

- If another fuel other than hydrogen is taken care of in the fuel cell, the performance step by step diminishes after some time because of catalyst debasement and electrolyte poisoning.

Solid Acid Fuel Cells

Solid Acid

Solid acids are substances that fall between common salt and regular acids (such as H_2SO_4) in terms of chemistry and characteristics (such as K_2SO_4). They typically consist of oxyanions joined together by hydrogen bonds, such as SO_4^{2-}.

Solid acids have ordered structures when temperatures are low [66]. Some solid acids go through transitions to extremely disordered super–protonic structures when the temperature rises (warm temperature), increasing the conductivity. The operating temperature for the solid acids is between $100\,^\circ$C to $300\,^\circ$C [87].

For example, at elevated temperature, due to the rotation of SO_4^{2-} ions, the structure of $CsHSO_4$ untie up. On a neighboring oxyanion, a proton on one of the oxygen ions can move towards an oxygen ion, which it is facilitating the proton transfer (Figure 3). According to the structural chemist, the four accessible areas for a proton on every oxyanion have gotten the same so the proton can decide to involve. Cesium hydrogen sulfate is a good solid acid that shows very promising protonic conductivity of 2.2×10^{-2} S-cm^{-1} at $240\,^\circ$C [88], and 4×10^{-2} S-cm^{-1} at $200\,^\circ$C [89], respectively.
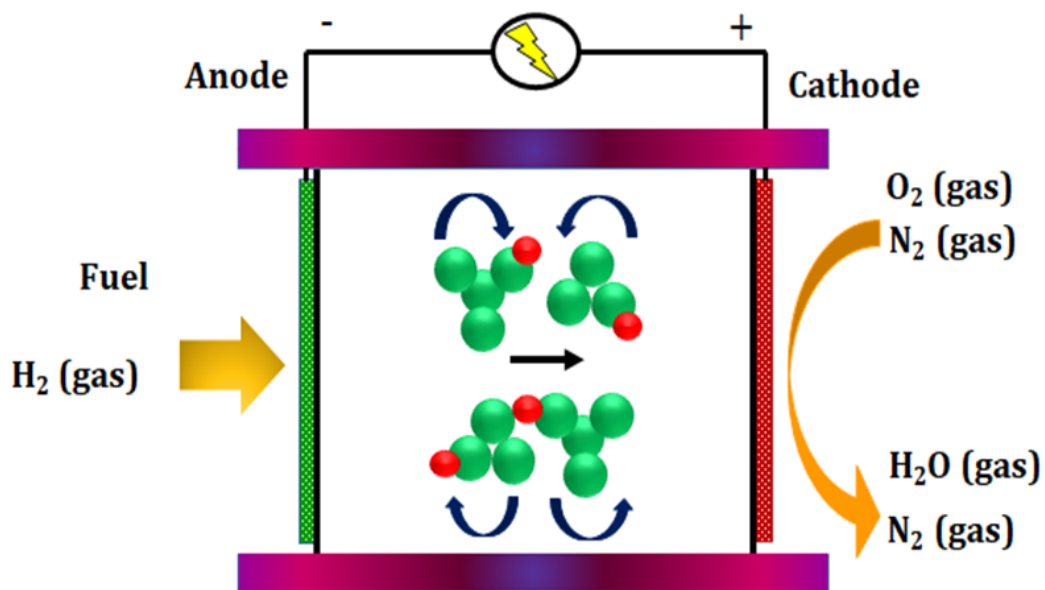

Figure 3. A proton transferring phenomena on a neighboring oxyanion, in which it is facilitating the exchange of proton [87].

A solid acid can be described by the following generic formula [90]:

$$M_a H_b (XO_t)_c \cdot nH_2O, \tag{4}$$

where

- M is one or more of the species that belong to the same phylum as Li, Be, Na, Mg, K, Ca, Rb, Sr, Cs, Ba, and NH_4^+ ;

- X is one or more of the species belonging to the group Si, P, S, As, Se, Te, Cr, and Mn, and;

- Rational numbers a, b, c, n, and t exist, with t preferable being 3 or 4 and $t \geq 0$ [91, 92].

Solid acid conductivity can be both protonic and electronic or purely protonic only. This is contingent upon the decision of the component for X in the chemical

equation[93]. Typically, acid and salt can be combined in the chemical equation of the solid acid.

Oxyanions, such as SO_4, SO_3, SeO_4, SeO_3, SiO_4, PO_4, or AsO_4, which are joined together by the O – H... O hydrogen bonds, contain strong acids. More than one type of XO_3 or XO_4 gathering, as well as more than one M species, may be present in the structure [94]. The usually utilized strong acids are Li^+, Na^+, K^+, Rb^+, and Cs^+ from Group I in the periodic table, PO_4^{3-}, AsO_4^{3-}, NH_4^+ joined with SO_4^{2-}, and transitional metal cations [95]. Nevertheless, at high temperatures, changes in the solid acid CDP's characteristics have been noted [88, 96–99]. There are some other types of solid acids known as binary solid acids or mixed solid acids. Hybrid compounds of $MHXO_4$ and MH_2ZO_4 make them up [100].

where, X is represented as S, Se

Z is presented as P, As and

M is signified as Li, Na, K, NH_4, Rb, Cs.

These combined strong acids exhibit qualities that are superior to those of single–salt strong acids, such as a wider range of the temperature for super–protonic conductivity and enhanced protonic conductivity at lower temperatures as a result of reduced activation enthalpy [101–103]. To increase the mechanical and thermal stability of the solid acids, different types of solid acids with high protonic conductivity, for instance, Heteropolyacids (HPAs), $Zr(HPO_4)_2$, SiO_2, TiO_2, Al_2O_3, ammonium polyphosphates [104–108] are combined to create heterogeneous doping.

Conduction mechanism of solid acids

When utilized as a proton-conducting membrane, solid acids have unique properties that are advantageous. The hydrogen ion is bonded between water molecules creating a link between R functional groups. These hydrogen bonds create the infinite chain by linking with oxy–anions of the solid acids. The mobility of the ions is not necessary for the proton transport mechanism. Because of this, solid acids do not require humidification, and their conductivity is mostly independent of moisture. It may be used above $100\,^\circ C$ since the solid acids are exempt from being humidified. A wide variety of 0D [109], 1D [110], 2D [111,112], and 3D [113] intermolecular networks of hydrogen bonds have been probed in solid acids. Figure 4 illustrates the proton transport system. When a proton binds to a conducting molecule, the hydrogen bond is then reoriented, and this is how proton transport occurs [114]. Reorienting a SO_4 tetrahedron in the superprotonic phase is thought to promote proton transport mechanism because it causes the hydrogen bond network to become disordered [115, 116]. At high temperatures, a super–protonic transition develops when the proton conductivity increases by two to four significant degrees.

Nevertheless, at higher temperatures, solid acids are often robust against thermal breakdown. For certain of the solid acids, the thermal disintegration temperature can reach $350\,^\circ C$. Additionally, the structure of the solid acids lends itself to advantages. Since solid acid is a condensed, inorganic material, it prevents
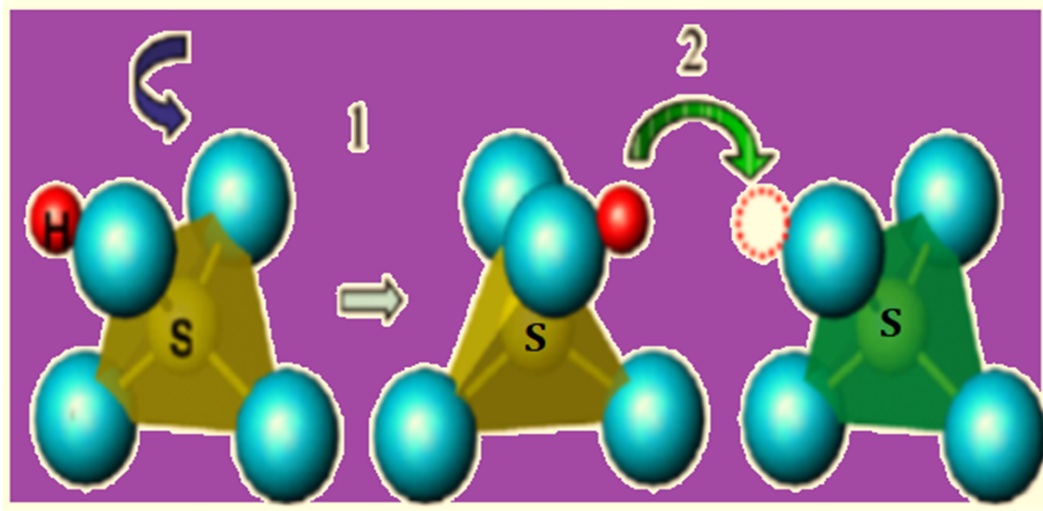
Figure 4. Mechanism for proton conduction of solid acid CsHSO$_4$ [59].

the passage of gases and other fluids that are prevalent in the electrochemical environment, such as gases and hydrocarbon liquids.

Characteristics of various types of solid acids

The proton transport mechanism in solid acids usually occurs through the Grotthuss transport mechanism [117], where protons can travel faster through liquids or aqueous [118]. In solid acids such as $NH_4H_2PO_4$ [119, 120], and KH_2PO_4 [121], the defects are created by dipole reorientation due to proton transport. Proton transportation also occurs through the vehicle mechanism where the proton is transported in polymer membranes. A hydrated proton aggregation flows across the aqueous environment as a single unit by a molecular diffusion process, as described by the vehicle mechanism [122]. Nafion generally acts as a polymer membrane in solid acid fuel cells. Nevertheless, certain materials, such those with large water contents and acidic stable hydrates, provide practical hurdles for proton transfer [123]. The fundamental characteristics of several materials utilized in the SAFC are displayed in Table 2.

Table 2.
The major characterizations of some materials used in the SAFC.

Electrolyte	Electrode	Operating temperature (°C)	Peak power density (mW cm^{-2})	Conductivity (S cm^{-1})	Ref.
MOA/CsH$_2$PO$_4$	-	25	38.5	2.1×10^{-4}	[124]
Tl$_3$H(SO$_4$)$_2$	Pt mesh (anode) and graphite (HOPG) (cathode)	40		2.0×10^{-5}	[125]
SiP$_2$O$_7$	Pd film	200		44×10^{-4}	[126]
Si$_3$(PO$_4$)$_4$	Pd film	200		57×10^{-4}	[126]
CsH$_5$(PO$_4$)$_2$/SiO$_2$	Pd (anode) and Pt (cathode)	140	8	2.3×10^{-4}	[127]
CsHSO$_4$/alumina	carbon paper (Pt black/C black)	160	2	-	[128]
CsH$_2$PO$_4$/SiP$_2$O$_7$	(Pt/C + CB) (anode) and Pt/C (cathode)	200	56		[33]
CsH$_5$(PO$_4$)$_2$/quartz fiber	Pt/C	200	105	3.3×10^{-2} (220)	[129]
CsH$_2$PO$_4$	Pt/CsH$_2$PO$_4$	250	-	-	[130]
CsH$_2$PO$_4$ or CDP	25 mg of CsH$_2$PO$_4$ + Pt on carbon with a mass ratio of 6:1 (anode), Pt@CsH$_2$PO$_4$ (cathode)	250	-	-	[131]
CsH$_2$PO$_4$	stainless steel (grade 304) mesh disc (anode), Pt/Pd (cathode)	250	-	-	[132]

According to Table 2, an H$_2$/O$_2$ fuel cell with the membrane attached was run at 200 °C, and for corresponding membrane thicknesses of 70 μm, an open-circuit voltage of 0.93 V and highest peak power densities of 105 mW cm^{-2} were attained [129].

Advantages and drawbacks of solid acids

Due to a combination of the following features, solid acids are ideal components for use as membranes in electrochemical devices:

- Arid environment with a preference for high conductivity;

- The regulation of conductivity allows for either pure proton conduction or mixed electron and proton-leading;

- Hydrocarbon liquids and gases cannot travel through it;

- Can operate at low temperatures (above $100\,^{\circ}$C);

- Relatively low cost.

Although there are many advantageous properties of solid acids, there is also a problem that can be experienced to actualize them in electrochemical gadgets. This is because many of them are soluble in water [133].

To overcome this problem, the solid acid can be disclosed with a supporting matrix. This matrix will provide mechanical support that protects it from the water environment and helps to increase chemical stability. Table 3 provides a summary of binder or matrix substances that may be used as mechanical support to safeguard the electrolyte for the solid acid.

Table 3.
List of binds or matrix [93].

| Polymer	Oxide or ceramic glass	Metals or semiconductors
Polyvinylidene flouride	SiO_2	Ag*
Polydicyclopentadiene	Al_2O_3	Au*
Polytetraflouroethelyne (Teflon)	MgO	Cu*
Polyether sulfone		
Polyether-ether ketone	Cordierite	Al*
Silicones (dimethyl)		Ni*
Polypyrrole*		Zn*
Polyaniline*		Graphite*, Silicon*

* indicating electronically conducting.

To offer a consistent slurry and distinct particles in the cathode and anode, the coating needs the binder's assistance in dispersing. To improve the mechanical strength and/or chemical stability of the membranes, an embodiment employs a structural binder or matrix material. In other implementations, the structural binder might be any number of different sorts of materials. A polymer, a ceramic, or an oxide glass, as shown in Table 3, can serve as the structural binder. For the electrodes to have adequate electrical conductivity, mechanical strength, and integrity, a polymer binder is required to bind the active material particles together [134]. Glass powders and substrates are not merely glued together

by ceramic or glass binder at low temperatures; rather, the binding activity is maintained up to the firing temperature [135]. Metal Binder is an adhesive that enables the bonding of materials such as rubber to metal surfaces such as steel and aluminum. A metal, such as Ag, Au, or Cu, and a proton conducting solid acid, such as $CsHSO_4$, $Cs_2(HSO_4)(H_2PO_4)$, $(NH_4)_3H(SO_4)_2$ or $CaNaHSiO_4$ are ground and combined. A structural binder from the category comprising electrically conducting carbon materials, polymers, ceramics, glasses, metals, and combinations thereof is also included in the proton conducting membrane [93].

Super–protonic conductors in solid acids

A material that can transfer protons from one location to another is referred to as a proton conductor. Low–temperature proton conductors, which operate at 20–$120\,^\circ C$ [136], intermediate–temperature proton conductors, which operate at 120–$250\,^\circ C$ [137], and high–temperature proton conductors, which operate at 500–$800\,^\circ C$ [138], are the three stages of the proton conduction mechanism. The Grotthuss mechanism is the most often used conducting mechanism. Only the protons exhibit long-range diffusion because the OH^- groups are reoriented and hop from OH^- to a neighboring oxide ion during the proton transfer. It demonstrates greater activation energy than the latter and necessitates the breakdown of the OH^- bond. According to defect chemistry, the following equation is where proton conducting species first appear [117, 139]:

$$H_2O_{(g)} + O_0^x + V_0^{\bullet\bullet} \rightarrow 2OH_0^\bullet, \tag{5}$$
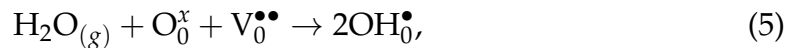
We may infer from equation (5) that a reduction in the partial pressure of water will cause the equilibrium to shift to the left, causing a fall in the concentration of $OH_0^\bullet$ and a corresponding drop in proton conductivity. Reactions (6) and (7) will be preferred in environments with high oxygen partial pressure:

$$V_0^{\bullet\bullet} + \frac{1}{2}O_2 = O_0^x + 2h^\bullet, \tag{6}$$

$$2OH_0^\bullet + \frac{1}{2}O_2 = 2O_0^x + H_2O + 2h^\bullet, \tag{7}$$
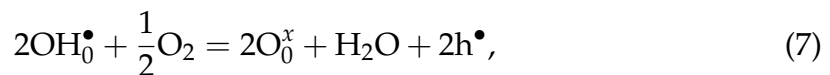
Due to the consumption of oxygen vacancies and OH^- groups brought on by a rise in the oxygen partial pressure, proton conductivity will decrease. In proton–conducting membranes, the solid acids exhibit the super–protonic property, which gives advantageous applications. When a first–order polymorphic phase transition, known as a super protonic transition, occurs at a high temperature in solid acid compounds, the proton conductivity increases by 2 to 4 orders of magnitude. The most extensively used perfluorinated sulfonated polymer, Nafion, is believed to be the best for proton–conducting materials [140]. Nevertheless, Liu et al. [141] claim that $\{H_6Bi_{12}O_{16}\}$ /GO composite membrane had superior proton conductivity than Nafion in an aqueous solution with a value of 0.564 Scm^{-1} at $80\,^\circ C$ and also shown good performance at sub–zero temperatures with a value of 2.17 104 Scm^{-1} at $40\,^\circ C$. At conditions of 97% RH, $\{H_6Bi_{12}O_{16}\}$ /GO

exhibited the Grotthuss mechanism. By determining that the activation energies (E_a) for pristine $\{H_6Bi_{12}O_{16}\}$ and $\{H_6Bi_{12}O_{16}\}$ /GO are approximately 0.52 eV and 0.24 eV from Arrhenius plots in the temperature range of 30–80 °C under 97% RH, respectively, the $\{H_6Bi_{12}O_{16}\}$ /GO composite showed super proton conductivity even at sub–zero temperatures and catalysed the decomposition of hydrogen peroxide.

In addition, according to Gorre et al. [142], the proton conductivity of the ImILSi3% membrane was discovered to be 0.219 Scm $^{-1}$ at 160 °C ($3 \approx 4$ fold higher than that of clean OPBI), making the mixed matrix PEMs naturally superconducting. By evaluating the crystalline ordering acquired from the PXRD, it is feasible to generate super proton conducting nanocomposite PEMs from the OPBI@ImILSi membranes that produce labile proton transport channels and operate as proton carriers when PA is added to the system.

The exquisite crystal structure of the potent acids may become disorganized at absolute pressure and temperature conditions. After this congestion, there is a conductivity that is enhanced and can range from 10^{-3} to 10^{-2} Ω^{-1} cm $^{-1}$ [66]. It is referred to as the super–protonic stage because of the fundamentally crowded state's strong proton conductivity. The rapid direction of the XO_4 or XO_3 gathering in this cycle promotes proton transport.

Super–protonic behavior can only occur in the monoclinic phases [143]. Numerous solid acids are thrust into the super–protonic state at the temperature between 50 °C to 150 °C at surrounding pressure.

Solid acid as an electrolyte

According to the Brnsted and Lewis definitions, a solid acid has a propensity to give a proton or take an electron pair [144]. Silica–based solid acids, zeolite–based solid acids, polymer–based solid acids, hydroxyapatite–based solid acids, zirconia–based solid acids, and carbon–based solid acids are some of the several types of solid acids [145]. But, for next–generation fuel cells, tetrahedral oxyanion–based solid acid proton conductors have drawn interest as the electrolytes. This family of materials, including $CsHSO_4$, $Rb_3H(SeO_4)_2$, and $(NH_4)3H(SO_4)_2$, demonstrate anhydrous proton transport (i.e., with the intricate formation and dissolution of hydrogen bonds between the charge–carrying solvent groups, the protons are moved between them [146, 147]) with conductivities on the order of 103 to 102 S-cm $^{-1}$ at mild temperatures (120–300 °C). Mostly, they are solid acids (or acid salt) [148]. The "superprotonic" transition, which occurs when proton conductors become extremely conductive at a specific temperature [88].

Solid acids such as CsH_2PO_4 and $CsHSO_4$ are an example of inorganic materials that have been known for their super–protonic conductivity at high temperatures. These inorganic materials operated at a temperature of roughly about 100 °C to 300 °C. There are three groups that are known as major solid acids that have been having a super protonic properties and have been classified as $CsHSO_4$, CsH_2PO_4, and $Rb_3H(SeO_4)_2$ [149, 150].

These materials have typical distinctive highlights during the super–protonic phase transition as follows:

- A sudden increase in conductivity;

- A huge endothermic contrast;

- An intense structure change brought about by the reorientation of the oxyanion gatherings, XO_4 (X=S, P, and Se);

- As well as during the cooling process, they have a large hysteresis [149].

There are two steps to explain the conduction mechanism for the compounds that have been mentioned above. Initially, a hydrogen connection between two nearby XO_4 tetrahedrons and proton displacement are involved. Furthermore, the reorientation of the XO_4 groups as a result of the breakage of the O–H–O hydrogen bonds [116, 151]. All the elements ($CsHSO_4$, CsH_2PO_4) belong to the monoclinic symmetry with different crystal structures and experienced the super–protonic transition and get into the phase about $127\,°C$ and $77\,°C$, respectively [149].

The solid acids compound $CsHSO_4$ was first investigated for evidence of principle in the applications of the fuel cells. This compound has a reasonably wide range in temperature between $100\,°C$ to $300\,°C$. During the investigation by the scientist, With significant mechanical contact with the layers of the electro-catalyst, the thickness of the electrolyte membrane was created to be in the range of 1 to 1.5 mm. The graph in Figure 5 has been obtained.
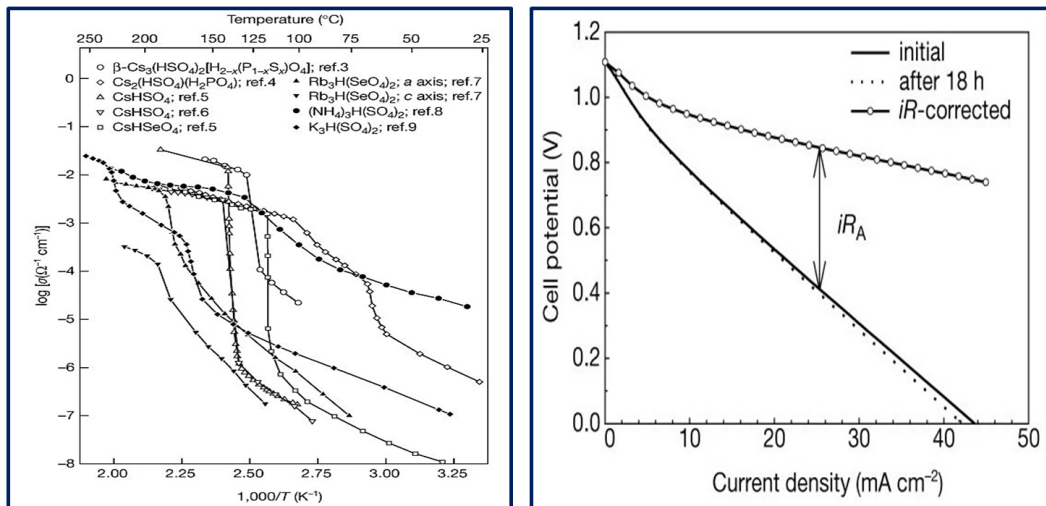

Figure 5. The Arrhenius plot of the solid acids and cell voltage against the current density polarization curve for CsH_2O_4 fuel cell [66].

The anode and cathode have been presented to H_2O–immersed H_2 and H_2O–saturated O_2 respectively and held at about $160\,°C$. The voltage decreases as the current density rise, which is apparent from the preceding diagram. This decrease may be brought on by the delayed charge transfer over the membrane, the resistance of the membrane as well as the thickness of the electrolyte that was employed in this study. The progress into the super–protonic stage might be either sharp or slow. This stage is set apart by an expansion in the conductivity, regularly by a few significant degrees. The solid acid is super–protonic and until

the degrading or dissolving temperature is achieved, the material maintains its high proton conductivity at the temperature over the changing temperature.

Despite the drop, the super–protonic properties of the $CsHSO_4$ transition phase were well acknowledged, different conductivities at $160\,^\circ$C were recorded. According to the experiment of the scientist, the slope for this combination at 1.37 mm in thickness is -17.1 Ω-cm^2 [66]. Figure 5 illustrates the perfect stability of solid acid in oxidizing circumstances. However, under a reduction atmosphere, there is weight reduction likely because of the slow sulfur decrease as indicated by reaction 8, which may likewise be answerable for the slight loss in fuel–cell execution by delivering the catalyst poison H_2S.

$$2CsHSO_4 + H_2 \rightarrow Cs_2SO_4 + H_2O + H_2S, \qquad (8)$$
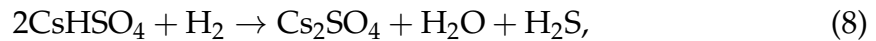
According to the preceding results (Figures 5), there are several benefits to using inorganic, water–liquefiable solid acids in H_2 or O_2 fuel cells since these materials produce larger OCVs, which might improve system efficiency as a whole. During high fuel utilization operation circumstances, the open–circuit voltage (OCV) predicted by the Nernst equation should be maintained at a high level providing a chance to create a system with great fuel efficiency and high power density as high conversion efficiency is known to be achieved by having a high open–circuit voltage [152]. Figure 5 has an OCV of 1.1 V which is the theoretical OCV values for fuel cell [153]. Moreover, because anhydrous electrolytes operate at a somewhat higher temperature than water, the catalyst may tolerate carbon monoxide more readily.

Improvement can be made to enhance the performance by having a thin membrane of the electrolytes and also putting in place a support structure that can keep liquid water from contaminating the electrolyte. It is been reported that the conductivity for $CsHSO_4$ at $160\,^\circ$C varies from $3.70 \times 10^{-3}\,\Omega^{-1}\,cm^{-1}$ to $2.08 \times 10^{-3}\,\Omega^{-1}\,cm^{-1}$ [66].

At room temperature, CsH_2PO_4 embraces the monoclinic structure, wherein the gatherings of XO_4 (PO_4) are connected through both the awry, single least hydrogen bonds and symmetric, double–minima bonds, which are formed between oxygen iotas of phosphate clusters, produce wrinkled two-dimensional layers of H_2PO_4, in the centre of which the Cs molecules are located, as seen in Figure 6 [88].

The reversal symmetry about the O(1)–O(1) hydrogen bond is removed, and the bond acquires asymmetry when CsH_2PO_4 undergoes a ferroelectric transition to a monoclinic symmetry of space group $P2_1$ during the cooling phase (with a solitary least). CsH_2PO_4 takes on a structure similar to CsCl at high temperatures. The cell is located near the Cs atoms and about in the middle of the primitive unit, where it is haphazardly oriented and adopts one of the six potential orientations. This can be observed in Figure 7.

As an electrolyte, CsH_2PO_4 has been investigated in SAFCs by scientists. The phosphate–based compound is not suffering from a reduction reaction to form solid phosphorus or gaseous H_xP species. This has been proved by the experiment that has been carried out under a hydrogen and oxygen atmosphere for the thermal analysis of CsH_2PO_4 by Sosina Haile et al. [94]. Although being
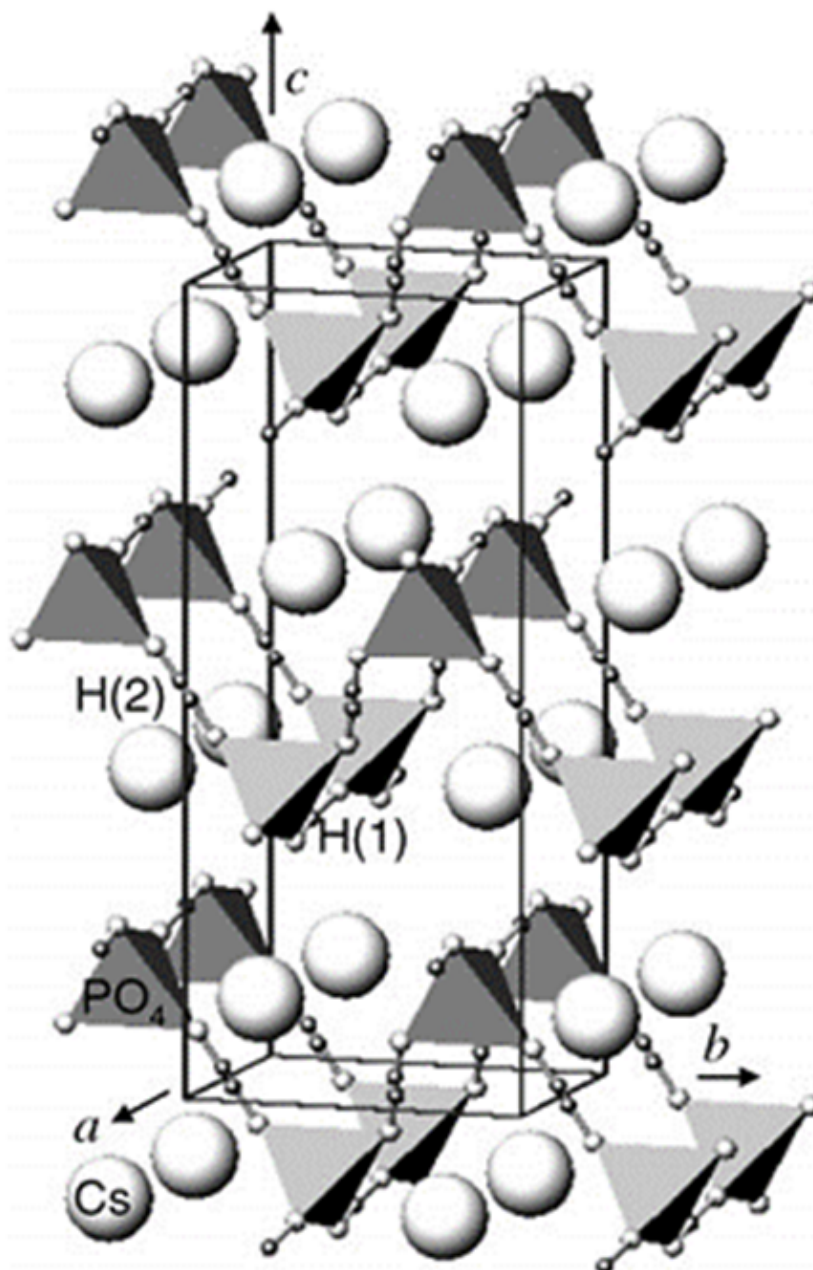
Figure 6. CsH_2PO_4 adopting the monoclinic structure at room temperature [88].

combined with the Pt catalyst seen in Figure 8, the experiment itself demonstrates that the molecule is not dependent on redox environments. Although being combined with the Pt catalyst, the chemical is not affected by the reducing or oxidizing environments.

At about a temperature of $223\,^\circ\mathrm{C}$, there is weight loss starts. Weight loss occurs because of dehydration. From the gas evolved analysis, there is no fragment of phosphate has been detected. Hence it has been proposed that dehydration occurs employing the development of formless hydrogen pyrophosphate and polyphosphate intermediates until the decay to $CsPO_3$ eventually happens. The reaction can be shown as equation (9) [94].
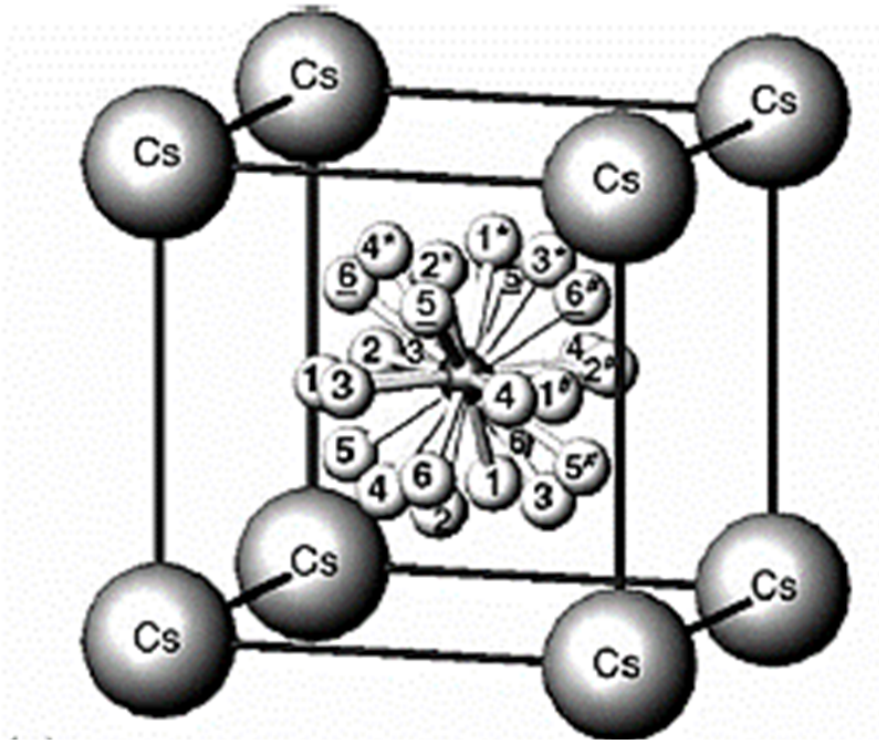
$$CsH_2PO_4(s) \rightarrow CsH_{2-2x}PO_4(s) + xH_2O(g), (0 \prec x \leq 1),\qquad(9)$$
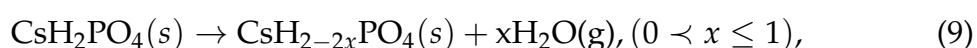
Figure 7. CsH_2PO_4 at high temperature adopts the CsCl–like structure [88].
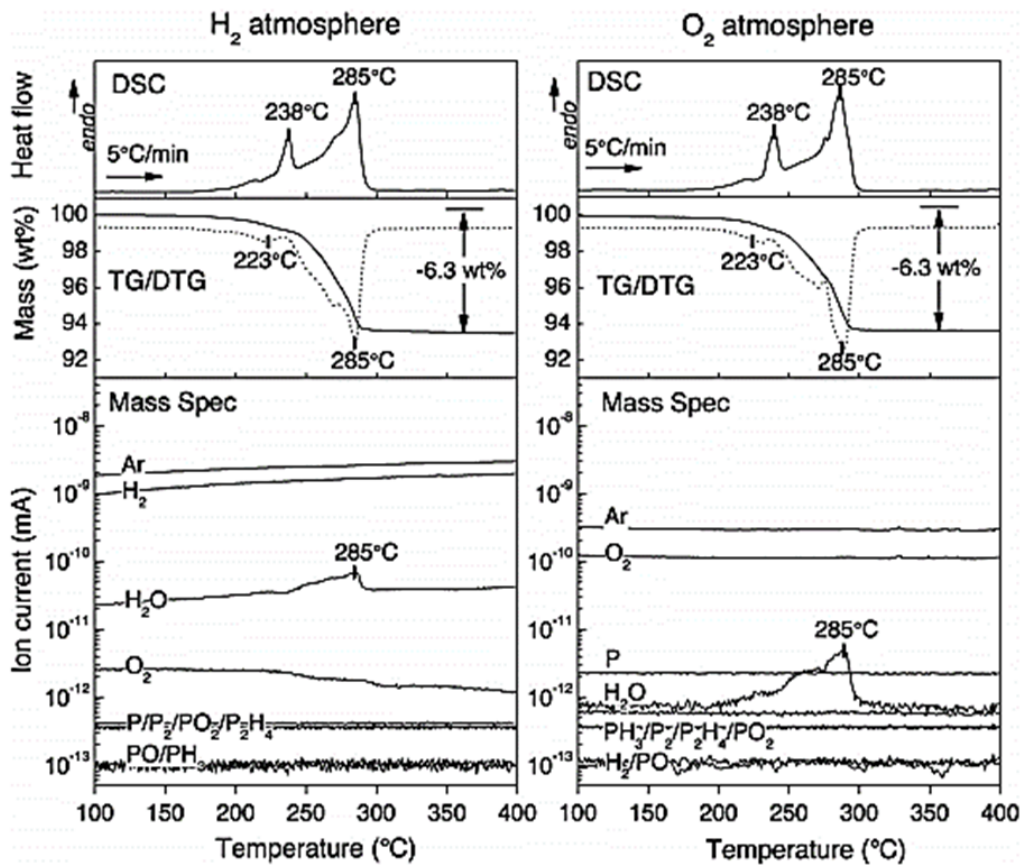

Figure 8. Thermal analysis of CsH_2PO_4 has been analyzed under hydrogen and oxygen atmospheres [94].

From the chemical equation, the main benefit of using this type of electrolyte (PO_4), there is no toxic gas has been formed compared to $CsHSO_4$. Consequently,

according to the experiment, humidification is necessary to maintain a good performance of the solid acid and to avoid the dehydration of the CsH_2PO_4 electrolyte. Using a Pt electrocatalyst at both electrodes and a 260 μm-thick CsH_2PO_4 electrolyte, a membrane electrode assembly (MEA) was created. Figure 9 demonstrates the cell's exceptional stability as the voltage rose from 0.44 V to 0.46 V. The cell was run at $235\,^\circ$C with humidified H_2 and O_2 gases flowing at 50 SCCM at the anode and cathode, respectively. At the anode and cathode, catalyst loading was at 50 SCCM and 260 m, respectively. Catalyst loading was 18 mg cm^{-2} Pt. PH_2O with an electrolyte thickness of 260 μm and a pressure of 0.30 atm. The maximum current density was 301 mA cm^{-2}, while the peak power density was 48.9 mW cm^{-2}.
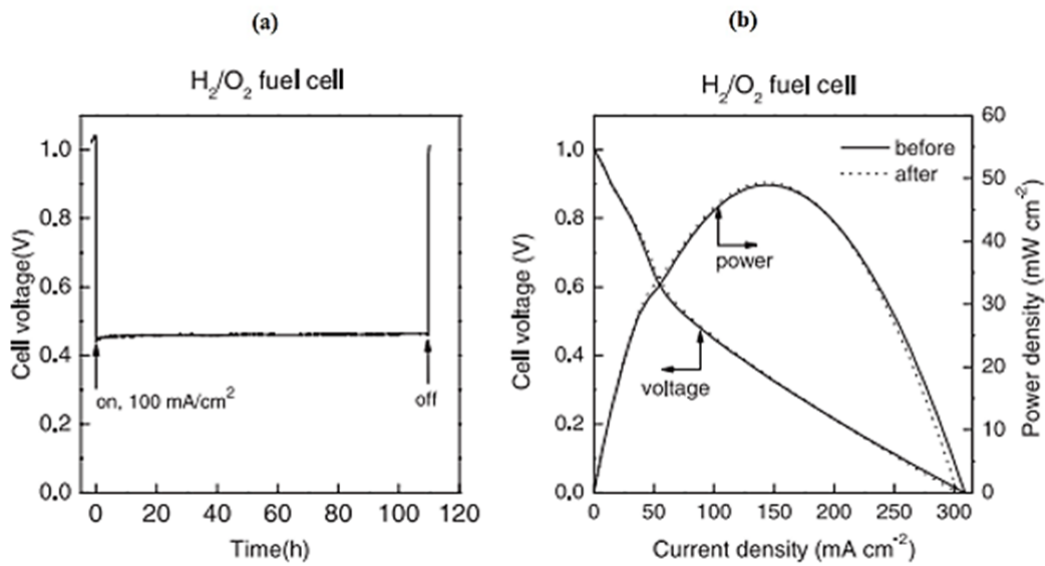

Figure 9. Execution of H_2 or O_2 fuel cells using a CsH_2PO_4 –based electrolyte [94].

The anode and cathode electrocatalysts were made from a combination of CsH_2PO_4, naphthalene, Pt black, and Pt supported on carbon (50 mass% Pt). Figure 10 illustrates the fuel cell polarization and power output curves from the four separate tests. The observed sample has maximum power density of 415 mW/cm^2 with a membrane thickness of, 260 μm. From the experiment for this compound, there is a limitation to the performance. The principal reason for this is electrolyte resistance. To improve this limitation, the performance of the cell is decreasing the thickness of the electrolyte. However, a stable performance could not be achieved for the thin membrane of the electrolyte [154].

Table 4 is to summarize the OCV, peak power density as well as cell voltage at every current drawn for four autonomous runs.
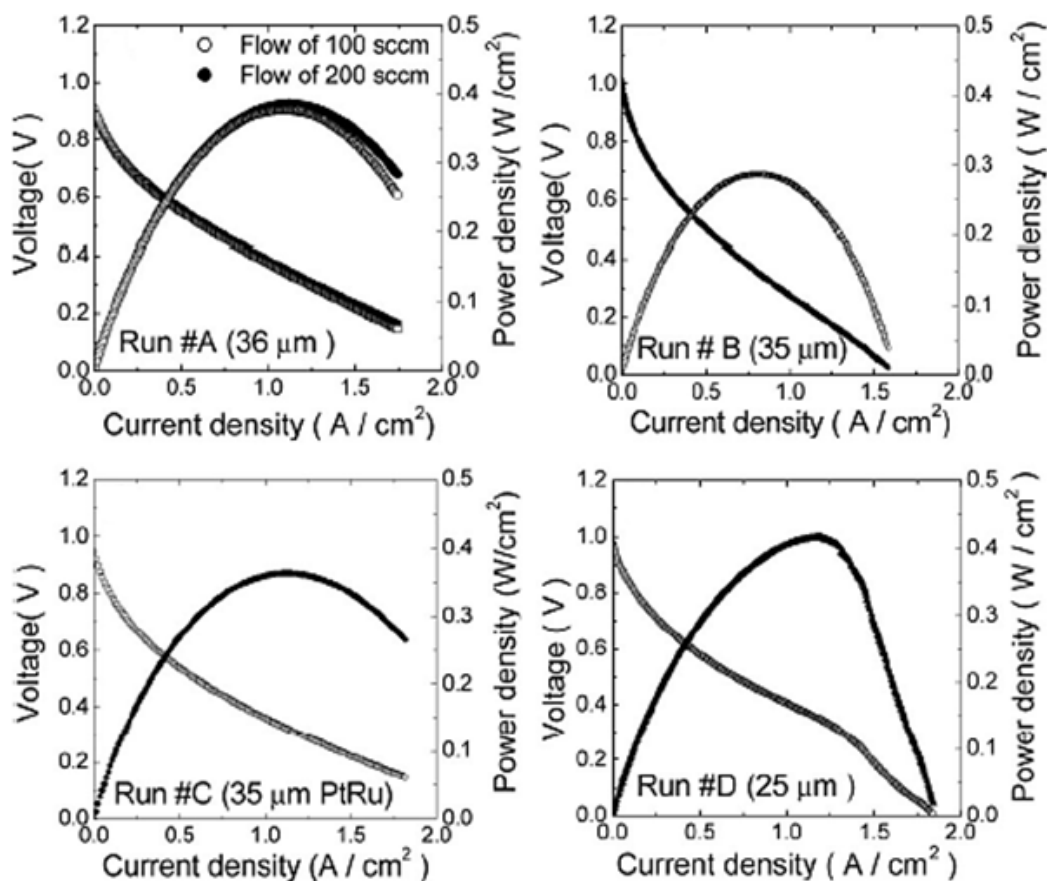
Figure 10. Power density curve corresponds with cell voltage attained from four independent tryouts [154].

Table 4.
Summarizes the peak power density, OCV, and cell voltage [154].

Run Number	Width of the electrolyte (μm)	OCV (V)	Peak power density (mW/cm^2)	Voltage V at 200 (mA/cm^2)	Voltage V at 400 (mA/cm^2)	Voltage V at 1000 (mA/cm^2)
A	36.00	0.91	385.00	0.70	0.60	0.38
B	35.00	1.01	287.00	0.70	0.56	0.27
C	35.00	0.95	362.00	0.71	0.58	0.36
D	25.00	0.98	415.00	0.75	0.63	0.40

With this unstable performance, the scientists assume that there are physical leaks through the material itself as the voltage loss across the thin membrane. The super–protonic solid acid is known to display superplastic conduct; with the end goal that the material is handily distorted by a slight mechanical power. This results from similar substance highlights of solid acid, the quick reorientation of tetrahedral oxyanion gatherings [154].

The wellspring of the voltage drop is expected to moderate electrocatalysis rates, slow particle transport over the electrolyte, and moderate mass dispersion through the electrodes. Along these lines, further expansions in power densities

for the strong acids energy units will require an improvement in expanding the electroanalytic movement. It has been reported that the conductivity of CsH_2PO_4 is 2.2×10^{-2} S/cm at $240°$C, with the area-specific resistance of 25 and 35 μm thick membranes 0.11 and 0.16 Ω/cm^2 [154]. Table 5 demonstrates how the solid acid performs when the thickness of the employed electrolytes' membrane is lowered and conductivity rises.

Table 5.
The conductivity of the solid acid electrolyte depending on the thickness of the membrane.

Electrolytes	Membrane with its thickness	Temperature (°C)	Conductivity	Reference
$CsHSO_4$	1.37 mm	160	$8 \times 10^{-3} \Omega^{-1} cm^{-1}$	[66]
CsH_2PO_4	25 μm	240	2.2×10^{-2} S.cm^{-1}	[154]
CsH_2PO_4	35 μm	240	2.2×10^{-2} S.cm^{-1}	[154]

The thermal behavior and conductivity of $MH(PO_3H)$ have also been studied, in which the M is Li^+, Na^+, K^+, Rb^+, Cs^+, and NH_4^+ [150].
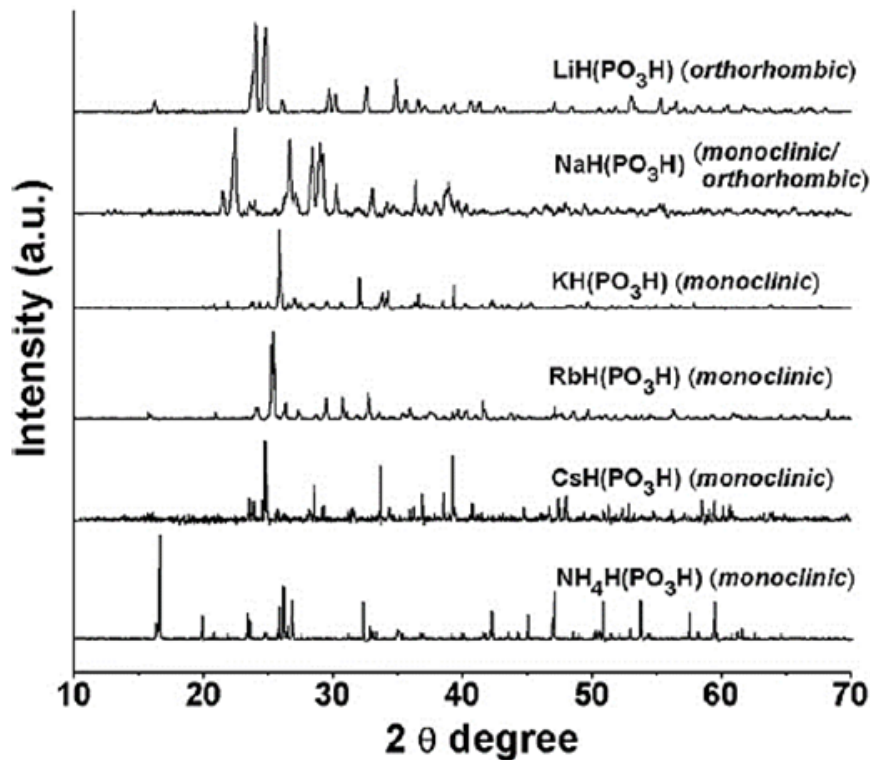

Figure 11. Patterns of XRD for $MH(PO_3H)$ phosphites [150].

Figure 11 above shows the structure of the $MH(PO_3H)$ at room temperature. Given what is evident, K^+, Rb^+, Cs^+, or NH_4^+ are all in monoclinic structure, and only Li^+ is totally in orthorhombic crystal structure while Na^+ can have either monoclinic or orthorhombic crystal structure at room temperature.

As the heat is applied to the compound $(MH(PO_3H)$, where M is Li^+, Na^+, K^+, Rb^+, Cs^+, or NH_4^+), everyone shows a super–protonic behavior except Li^+. Figure 12 depicts this with a super–protonic transition denoted with ST.
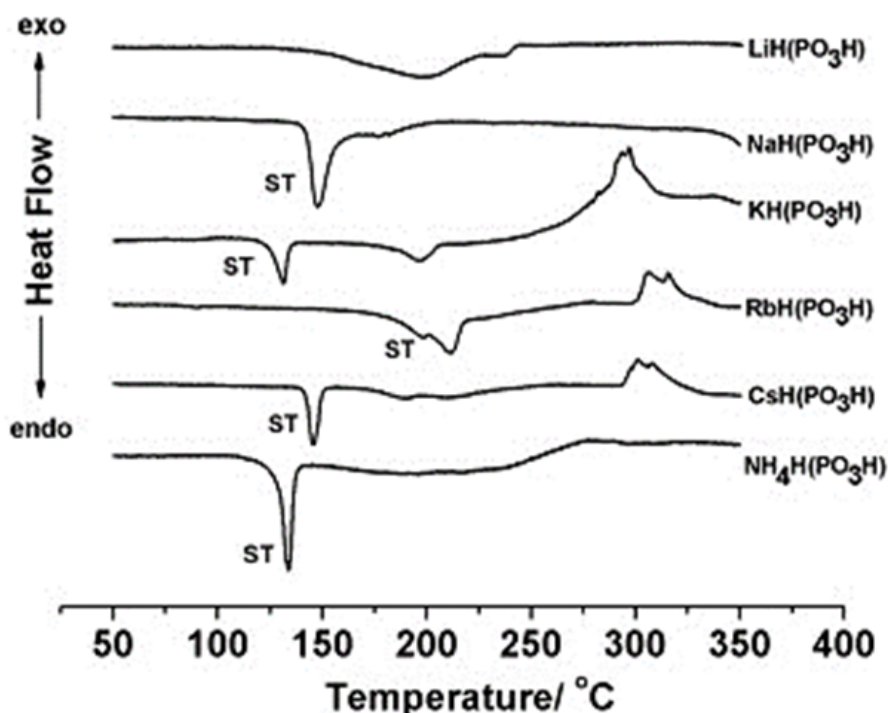
Figure 12. Thermal analysis of phosphite from DTA measurement where superprotonic transition is labeled with ST [150].

Figure 13 illustrates the impact of temperature on the $(MH(PO_3H))$ phosphites' proton conductivity. In agreement with the ST-labeled thermal events picked up by differential thermal analysis, the conductivities of the monoclinic phosphates are observed to drastically rise at the super–protonic transition temperatures (DTA).

According to the information acquired, all monoclinic phases of $(MH(PO_3H))$ with M as Na^+, K^+, Rb^+, Cs^+, and NH_4^+ display super protonic conduct after warming, much like $CsH(PO_3H)$ does. Only $KH(PO_3H)$ and $CsH(PO_3H)$ have been employed to show the viability of dynamic drying out after structural phase change [110, 155]. Orthorhombic $LiH(PO_3H)$ does not exhibit super protonic conduct, in contrast to the monoclinic dihydrogen phosphates, and before thermal degradation, its conductivity is usually less than 10^{-8} Ω^{-1} cm^{-1} [150].

$KH(PO_3H)$ and $CsH(PO_3H)$, the two substances that cycle the warmest, are the most stable. Unexpectedly, as the temperature rises, $KH(PO_3H)$ conductivity rises 1.4×10^{-7} Ω^{-1} cm^{-1} at $80\,^\circ$C to 3.8×10^{-3} Ω^{-1} cm^{-1} at $135\,^\circ$C, implying above the super protonic change temperature. At $140\,^\circ$C, it is estimated that the proton conductivity will be 4.2×10^{-3} Ω^{-1} cm^{-1} at $140\,^\circ$C. At $65\,^\circ$C, the conductivity decreases with cooling to 5.2×10^{-6} Ω^{-1} cm^{-1}.

The following cycle showed the hysteresis conduct of the conductivity displayed in Figure 14, with a slight loss of conductivity over the super protonic change temperature due to drying-out influences.

Because of differences in the thermal histories of the samples used, the super–protonic conductivity observed for $CsH(PO_3H)$ is found to be considerably more modest (3×10^{-3} Ω^{-1} cm^{-1} at $160\,^\circ$C) for this salt[150]. $KH(PO_3H)$ possesses a super–protonic conductivity exceeding $135\,^\circ$C in its high-temperature solid phase. Its conductivity is comparable to that of famous $CsHSO_4$, whose super–
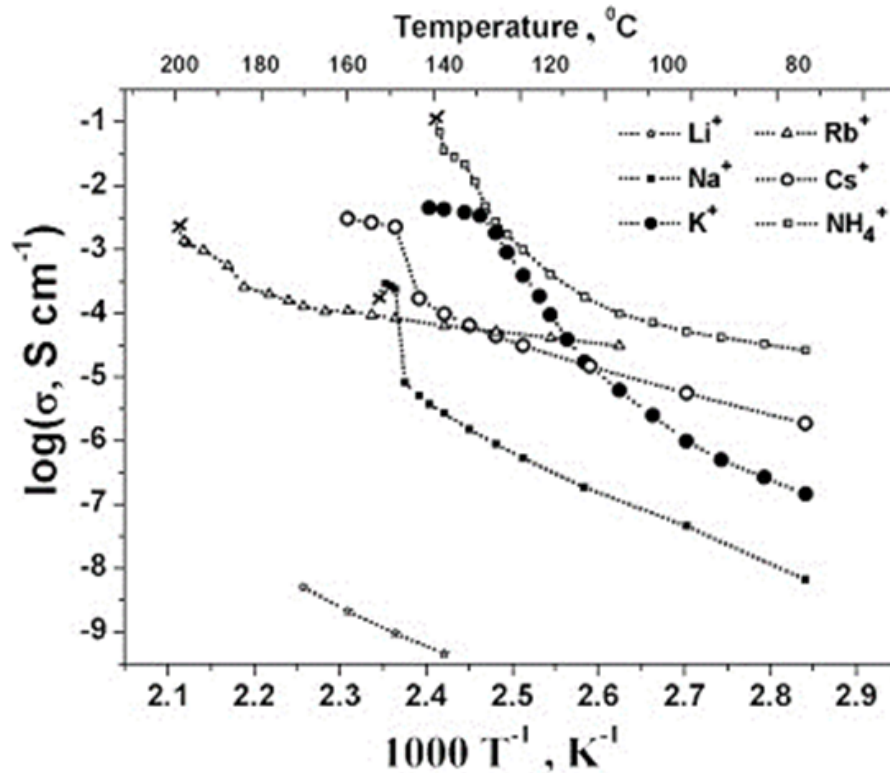
Figure 13. Arrhenius plot of phases $MH(PO_3H)$ proton conductivity. Estimates were made under a dry N_2 environment. Crosses indicate when heat breakdown causes a considerable decrease in conductivity [150].
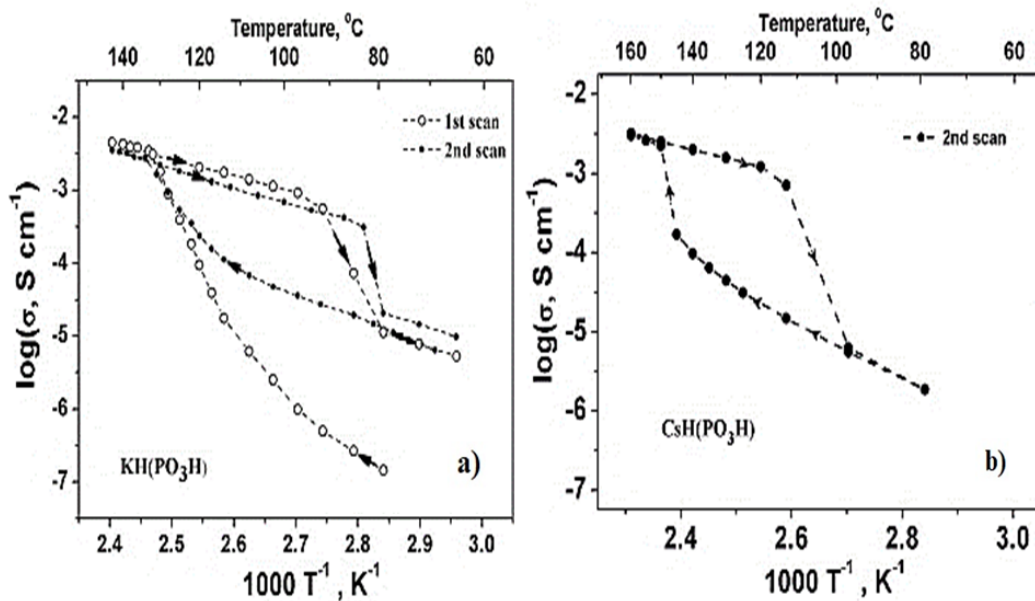

Figure 14. Conductivity of (a) $KH(PO_3H)$ and (b) $CsH(PO_3H)$ on thermal cycling in which estimation is taken in an arid N_2 environment [150].

protonic transition temperature is $141\,^\circ C$ [66]. $KH(PO_3H)$ is understood to be more stable in a hydrogen environment compared to $CsHSO_4$. $KH(PO_3H)$, which exhibits super–protonic behavior, is susceptible to delayed drying out in a dry nitrogen environment [66, 150].

Solid acid is the chemical intermediate between typical salts and standard acids. Solid acid has been used in Solid acid fuel cells as it has super protonic

behavior at slightly elevated temperatures or warm temperatures. This super protonic behavior because it increases in conductivity as the solid acid undergoes transitions to the disorderly structure.

In the case of $CsHSO_4$ (Figure 15) that has been experimented with by Haile, the HSO_4^- group forms a tetrahedron with at each corner oxygen and hydrogen sitting on one of the oxygen. At room temperature, all the sulfate groups have a fixed orientation. As the temperature rises, the sulfate groups reorient and cause disorder, as the hydrogen position also changes at this elevated temperature. Occasionally, the proton transfers from one sulfate to the other as the sulfate group rotates freely. Super–protonic phase is the result of the abrupt, several–orders–of–magnitude increase in conductivity that occurs as these materials move through this transition.
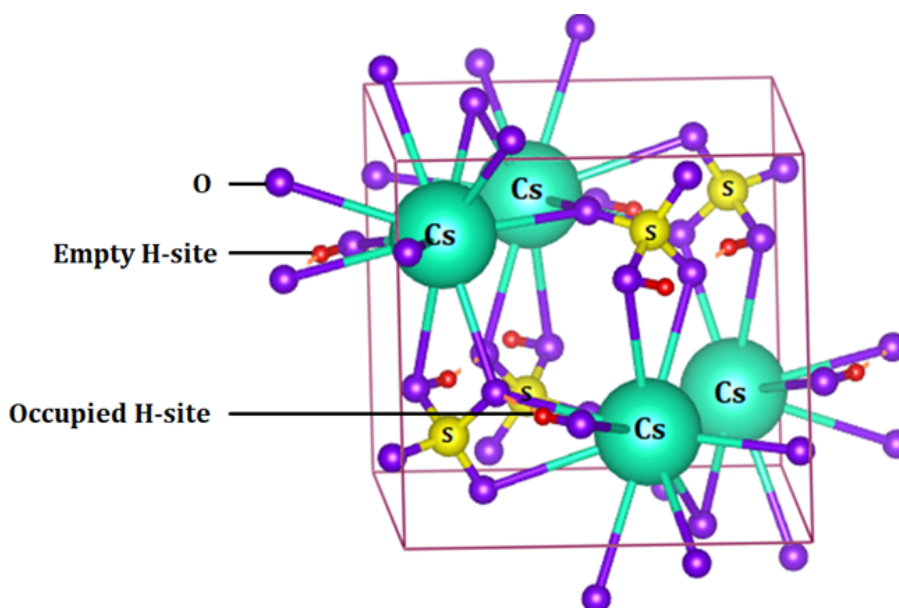

Figure 15. Structural disorder of $CsHSO_4$ [156].

Conductivity esteems for the salts are comparable to the Nafion and other polymer electrolytes, however, at somewhat higher temperatures. Given the extremely high conductivity of solid acids and the mode of proton transfer, the presence of water is not required and subsequently does not depend on it. This reality makes them appealing to the fuel cell as the electrolytes.

SAFCs provide a few noteworthy differences from PEMFCs, including the following:

- Auxiliary humidification equipment can be eliminated as the proton transport is anhydrous;

- Results in measurably higher open-circuit voltages as the solid acid is completely impermeable to H_2 and O_2;

- direct methanol fuel cell operation is possible thanks to perfect methanol impermeability; and

- the Pt catalyst performs better when operated at a warm temperature, which lowers the amount of hydrogen gas that needs to be purified (improves the "CO tolerance" of the catalyst).

The advantages of the super–protonic solid acid fuel cell over the polymer electrolyte membrane (PEMFC) can be summarized in Table 6.

Table 6.
Comparison between SAFC and PEMFC.

	SAFC	PEMFC
Conductivity	0.05 S/cm	0.1 S/cm
Pressure system	1 atm	3 atm
Impermeable to fuels	None	Methanol and Ethanol
Operating temperature	100–300°C	25–90°C
CO tolerance	1-2%	Less than 100ppm
Water management system	Water condensation	Water re-circulation under pressure
Heat management	Maintain the operating temperature	Must keep system below 100°C

Apart from being able to operate at elevated temperatures, SAFCs have two other distinct benefits over PEMFCs:

- Impermeable to gases (no loss of gas through unwanted cross–over);

- Rather than inefficiently carrying over excess water molecules, as is the case with PEMFC, they transport bare protons through the membrane.

As mentioned in the literature review, the $CsHSO_4$ is the first investigated to prove the principle of the fuel cell application. However, the sulfate and selenite compounds react with hydrogen in the anode chamber and produce hydrogen sulfate as the by-product which is poisonous, this reaction occurs mainly in the occurrence of the catalyst of the fuel cell. This electrolyte, therefore, is not suitable for long-term operation.

The investigation of CsH_2PO_4–another electrolyte–followed. It can operate steadily for more than a hundred hours of continuous operation when hydrostatic pressure and water partial pressure are utilized as tools to suppress any disintegration or lack of hydration processes.

Figure 16 illustrates the super protonic transition, which occurs at $230°C$ and 1 atm of total pressure. The compound is balanced out against aridness at fractional water pressure over the blue curve. Typical fuel cell operating conditions are depicted by the yellow dab. A partial water pressure of 0.3 atm is adequate to stabilize CsH_2PO_4 up to a temperature of $250°C$ beyond the super protonic transition, according to the initial estimates of the thermodynamics of the parchedness processes.

Similar to this, if the ambient water partial pressure is more than 0.12 atm, it is possible to really produce CsH_2PO_4 in fuel cells that operate at a temperature of around 250 Similar to this, if the ambient water partial pressure is more than
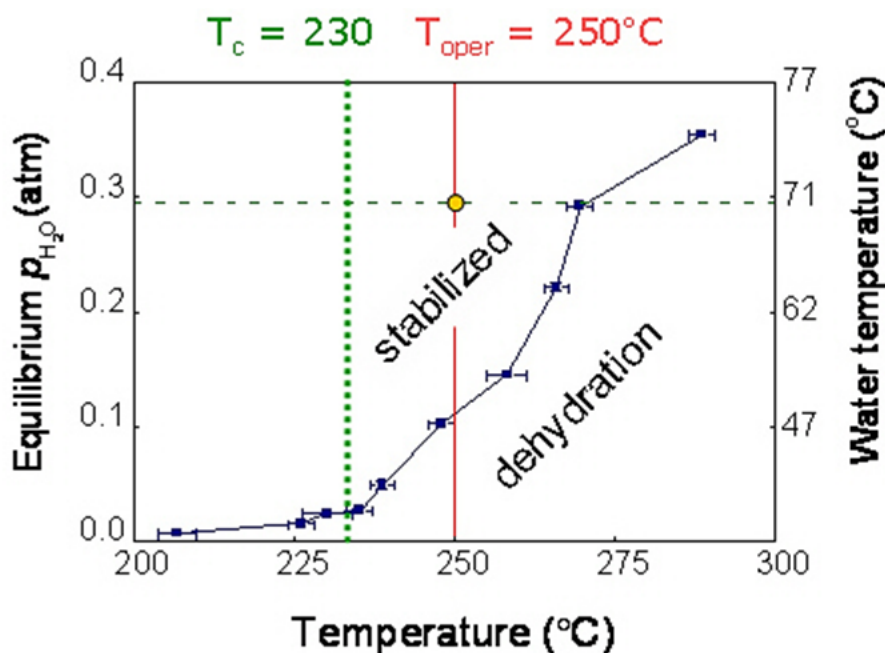
Figure 16. Behavior of CsH_2PO_4 under dehydration [157].

0.12 atm, it is possible to really produce CsH_2PO_4 in fuel cells that operate at a temperature of around $250\,^\circ$C. These findings further explain why there is such a discrepancy in the text on the conductivity of CsH_2PO_4. In certain places, but not all, the humidity levels required to balance CsH_2PO_4 are routinely met.

The performance of the solid acid fuel cell is significantly influenced by the thickness of the electrolyte membrane as well. As the thicker the membrane, the performance will be degrading due to the membrane will act as the resistance and slow down the transfer of the ions across it. Furthermore, an unstable version will also be experienced if the membrane of the electrolyte is too thin due to the material can be easily deformed by the mechanical force from the super–protonic or superplastic behavior. Therefore it is suggested to experiment with the thickness of the electrolyte membrane between 35 µm and less than 1.3 mm to see the performance and conductivity of the fuel cell.

Conclusions

Solid acids exhibit super–protonic conductivity as a result of a proton transport process via the Grotthus proton transport mechanism. Due to their super protonic characteristic and durability at high temperatures, solid acids are a suitable material for the electrolyte in fuel cell applications. high–temperature. The Grotthus mechanism of proton transport, which occurs at the high temperature phase transition and causes an anomaly in conductivity, is responsible for the super protonic characteristic of solid acids. Thus, fuel cells may certainly use solid–state proton conductors, and the importance of protonics has been expanded to the intermediate temperature range. One of the most promising sloid electrolytes is $CsHSO_4$, which loosens up to let the SO_4^{2-} ions to spin, allowing a proton on one oxygen ion to approach an oxygen ion on a nearby oxyanion, promoting

proton transfer. To sum up, a number of elements influence or help the solid acid fuel cell function well:

1. As the thicker the membrane, the performance will be degrading due to the membrane will act as the resistance and slow down the transfer of the ions across it. On the other hand, unstable performance will also be experienced if the membrane of the electrolyte is too thin due to the material can be easily deformed by the mechanical force from the super-protonic or superplastic behavior;

2. The choices of electrolytes also affect the performance of the solid acids;

3. Only the monoclinic crystal structure can undergo super-protonic transition;

4. Water partial pressure is also essential to obtain a stable performance of the solid acid, especially for some dry places that apply this method;

5. The electrolyte is in the solid state making it more efficient compared to the other electrolyte in the form of liquid as corrosion resistance can be built.

Acknowledgments

Conflict of interest

The authors state that they are clear of any financial conflicts of interest.

References

[1] Shammya Afroze et al., Int. J. Integr. Eng. **12** (2020) 245–256. [*CrossRef*]
[2] A.V. Nikonov et al., Eurasian J. Phys. Funct. Mater. **2** (2018) 274–292. [*CrossRef*]
[3] P. Duffy et al., in: Issues Environ. Sci. Technol., Royal Society of Chemistry (2019) 1–41. [*CrossRef*]
[4] M.S. Reza et al., Chem. Eng. Technol. **46**(3) (2022) 420–434. [*CrossRef*]
[5] C. Zou et al., Nat. Gas Ind. B **3** (2016) 1–11. [*CrossRef*]
[6] L.A. Omeiza et al., Energies **16**(4) (2023) 1876. [*CrossRef*]
[7] M. Beigzadeh et al., J. Clean. Prod. **280** (2021) 124383. [*CrossRef*]
[8] M.S. Reza et al., Arab J. Basic Appl. Sci. **27** (2020) 208–238. [*CrossRef*]
[9] Z.H. Lee et al., Renew. Sustain. Energy Rev. **28** (2013) 71–81. [*CrossRef*]
[10] W.H. Liew et al., J. Clean. Prod. **71** (2014) 11–29. [*CrossRef*]
[11] M.S. Reza et al., Sustainability **15** (2023) 1643. [*CrossRef*]
[12] M.S. Reza et al., Sustainability **14** (2022) 1203. [*CrossRef*]
[13] T.-Y. Lin et al., Gas Sci. Eng. **110** (2023) 204902. [*CrossRef*]

[14] S. Sabzpoushan et al., Energy Sci. Eng. **8** (2020) 3575–3587. [*CrossRef*]

[15] European Parliament, Directorate-General for Parliamentary Research Services et al., Towards a circular economy: waste management in the EU, European Parliament (2018). [*CrossRef*]

[16] S. Manafi et al., J. Nanomater. **2012** (2012) 803546. [*CrossRef*]

[17] M.S. Reza et al., Energy, Ecol. Environ. **5** (2020) 118–133. [*CrossRef*]

[18] J. Rissman et al., Appl. Energy **266** (2020) 114848. [*CrossRef*]

[19] S. Afroze et al., IET Conf. Publ., Institution of Engineering and Technology (2018) 4 p. [*CrossRef*]

[20] H. Forootan Fard et al., Int. J. Hydrogen Energy **45** (2020) 25307–25316. [*CrossRef*]

[21] M. Beigzadeh et al., Appl. Therm. Eng. **166** (2020) 114707. [*CrossRef*]

[22] M.A. Hannan et al., Int. J. Hydrogen Energy **47** (2022) 39523–39548. [*CrossRef*]

[23] M.J.B. Kabeyi et al., Front. Energy Res. **9** (2022) 1–45. [*CrossRef*]

[24] F. Wu et al., Chem. Soc. Rev. **49** (2020) 1569–1614. [*CrossRef*]

[25] M. Ma et al., Mater. Chem. Front. (2023). [*CrossRef*]

[26] C.D. Reynolds et al., Mater. Des. **209** (2021) 109971. [*CrossRef*]

[27] J. Lin et al., Energy Environ. Mater. **5** (2022) 133–156. [*CrossRef*]

[28] C. Xiong et al., SmartMat **4** (2023) 1–36. [*CrossRef*]

[29] A. Afif et al., J. Energy Storage **25** (2019) 100852. [*CrossRef*]

[30] S. Afroze et al., Int. J. Hydrogen Energy (2022). [*CrossRef*]

[31] T.H. Lee et al., J. Power Sources **331** (2016) 495–506. [*CrossRef*]

[32] A.V. Nikonov et al., J. Alloys Compd. **865** (2021) 158898. [*CrossRef*]

[33] S. Tada et al., Int. J. Hydrogen Energy **44** (2019) 26545–26553. [*CrossRef*]

[34] X.R. Wang et al., Int. J. Hydrogen Energy **46** (2021) 12206–12229. [*CrossRef*]

[35] S. Cavaliere et al., Energy Environ. Sci. **4** (2011) 4761–4785. [*CrossRef*]

[36] K. Sharma et al., J. Energy Storage **21** (2019) 801–825. [*CrossRef*]

[37] A.M. Abdalla et al., Front. Energy **14** (2018) 359–382. [*CrossRef*]

[38] R. Borah et al., Mater. Today Adv. **6** (2020) 100046. [*CrossRef*]

[39] R.T. Yadlapalli et al., J. Energy Storage **49** (2022) 104194. [*CrossRef*]

[40] B.C.H. Steele et al., Nature **414** (2001) 345–352. [*CrossRef*]

[41] M.A. Abdelkareem et al., J. Sci. Adv. Mater. Devices **7** (2022) 100465. [*CrossRef*]

[42] M.-R. Gao et al., Chem. Soc. Rev. **42** (2013) 2986–3017. [*CrossRef*]

[43] S.K. Dash et al., Sustainability **14** (2022) 8285. [*CrossRef*]

[44] W. Apollon et al., Biomass and Bioenergy **148** (2021) 106028. [*CrossRef*]

[45] G. Shen et al., Nat. Commun. **11** (2020) 1–10. [*CrossRef*]

[46] M.K. Debe et al., Nature **486** (2012) 43–51. [*CrossRef*]

[47] SAFCell - Solid Acid Fuel Cells convert fuel into electricity. [*Web Link*] (accessed Oct. 18, 2020).

[48] S. Afroze et al., Front. Energy **13** (2019) 770–797. [*CrossRef*]

[49] S. Afroze et al., Ceramics International **47** (2021) 541–546. [*CrossRef*]

[50] S. Afroze et al., Mater. Lett. **261** (2020) 127126. [*CrossRef*]

[51] S. Afroze et al., Int. J. Integr. Eng. **12** (2020) 245–256. [*CrossRef*]

[52] L. Xing et al., Energy **177** (2019) 445–464. [*CrossRef*]

[53] K. Vignarooban et al., Chinese J. Catal. **36** (2015) 458–472. [*CrossRef*]

[54] J. Millichamp et al., J. Power Sources **284** (2015) 305–320. [*CrossRef*]

[55] K.A. Kuterbekov et al., Eurasian J. Phys. Funct. Mater. **1** (2017) 48–51. [*CrossRef*]

[56] Y.M.A. Welaya et al., Int. J. Nav. Archit. Ocean Eng. **3** (2011) 141–149. [*CrossRef*]

[57] S. Mekhilef et al., Renew. Sustain. Energy Rev. **16** (2012) 981–989. [*CrossRef*]

[58] N. Radenahmad et al., Renew. Sustain. Energy Rev. **57** (2016) 1347–1358. [*CrossRef*]

[59] S.M. Haile et al., Mater. Today **6** (2003) 24–29. [*CrossRef*]

[60] Y. Manoharan et al., Appl. Sci. **9** (2019). [*CrossRef*]

[61] S.M.H. Rahman, Synthesis, Structure and Proton Conduction of Substituted BaTiO$_3$ and BaZrO$_3$ Perovskites (Chalmers University of Technology, 2013) [*Web Link*]

[62] Collecting the History of Proton Exchange Membrane Fuel Cells. [*Web Link*] (accessed Oct. 19, 2020)

[63] R. Omrani et al., Int. J. Energy Res. **43** (2019) 7496–7507. [*CrossRef*]

[64] I. Dincer et al., Int. J. Energy Res. **31** (2007) 29–55. [*CrossRef*]

[65] B. Yang et al., Mater. Res. Bull. **38** (2003) 691–698. [*CrossRef*]

[66] S.M. Haile et al., Nature **410** (2001) 910–913. [*CrossRef*]

[67] A.G. Olabi et al., Energy **214** (2020) 118955. [*CrossRef*]

[68] F. Wang et al., Appl. Energy **275** (2020) 115342. [*CrossRef*]

[69] BEHAVIOUR OF ACIDS, ALKALIS AND SALTS, in: Abridged Science for High School Students **2** (1966) 26-1–26–10. [*CrossRef*]

[70] S.D. Priya et al., J. Electrochem. Sci. Technol. **11** (2020) 99–116. [*CrossRef*]

[71] J.B. Goodenough et al., J. Power Sources **173** (2007) 1–10. [*CrossRef*]

[72] R.N. Basu et al., Recent Trends Fuel Cell Sci. Technol. (2007) 286–331. [*CrossRef*]

[73] Fuel Cells. [*Web Link*] (Accessed: Nov. 18, 2018)

[74] E. Ogungbemi et al., Energy **172** (2019) 155–172. [*CrossRef*]

[75] N.H. Jawad et al., Sustainability **14** (2022) 14653. [*CrossRef*]

[76] H.S. Thiam et al., Int. J. Hydrogen Energy **36** (2011) 3187–3205. [*CrossRef*]

[77] H. Yu et al., Ref. Modul. Mater. Sci. Mater. Eng. (2016) 1–15. [*CrossRef*]

[78] K. Joon et al., J. Power Sources **61** (1996) 129–133. [*CrossRef*]

[79] J. Garche and L. Jorissen, Electrochem. Soc. Interface (2015) 39–43. [*Web Link*] (Accessed: Nov. 18, 2018)

[80] R. Mucke et al., J. Am. Ceram. Soc. **92** (2009) S95–S102. [*CrossRef*]

[81] M. Liang et al., Chem. Eng. J. **420** (2021) 127717. [*CrossRef*]

[82] A.K. Azad et al., Sci. Rep. **11** (2021) 19382. [*CrossRef*]

[83] A. Dubois et al., J. Power Sources **369** (2017) 65–77. [*CrossRef*]

[84] C.R.I. Chisholm et al., Electrochem. Soc. Interface **18** (2009) 53–59. [*CrossRef*]

[85] J. Wang et al., Engineering **4** (2018) 352–360. [*CrossRef*]

[86] O. Gonzalez-Espasandin et al., Sci. World J. 2014 (2014) 497642. [*CrossRef*]

[87] T. Norby et al., Nature **410** (2001) 877–878. [*CrossRef*]

[88] S.M. Haile et al., Faraday Discuss. **134** (2007) 17-39. [*CrossRef*]

[89] C. Yang et al., J. Power Sources **103** (2001) 1–9. [*CrossRef*]

[90] G.P. Pez et al., European Patent (2007). [*Web Link*]

[91] Wing Kee Chan et al., Structure and Dynamics of Hydrogen in Nanocomposite Solid Acids for Fuel Cell Applications (Delft University of Technology, 2011). [*Web Link*]

[92] N. Mohammad et al., Malaysian J. Anal. Sci. **20** (2016) 633–641. [*CrossRef*]

[93] S. Afroze et al., Int. J. Chem. Eng. **2021** (2021) 5539048. [*CrossRef*]

[94] D.A. Boysen et al., Science **303** (2004) 68–70. [*CrossRef*]

[95] A.C. Dupuis et al., Prog. Mater. Sci. **56** (2011) 289–327. [*CrossRef*]

[96] E. Rapoport et al., J. Solid State Chem. **24** (1978) 423–433. [*CrossRef*]

[97] B. Metcalfe et al., Thermochim. Acta Acta, **24** (1978) 149–153. [*CrossRef*]

[98] L.C. Gupta et al., Thermochim. Acta **42** (1980) 85–90. [*CrossRef*]

[99] A.I. Baranov et al., Ferroelectrics **81** (1988) 183–186. [*CrossRef*]

[100] C.R.I. Chisholm, Superprotonic Phase Transitions in Solid Acids: Parameters affecting the presence and stability of superprotonic transitions in the MH_nXO_4 family of compounds (X=S, Se, P, As; M=Li, Na, K, NH4, Rb, Cs) (California Institute of Technology, 2003) [*Web Link*]

[101] A.I. Baranov et al., Solid State Ionics **176** (2005) 2871–2874. [*CrossRef*]

[102] V. V. Martsinkevich et al., Solid State Ionics **225** (2012) 236–240. [*CrossRef*]

[103] S.M. Gadzhiev et al., Russ. J. Electrochem. 45 (2009) 215–220. [*CrossRef*]

[104] A. Corma et al., Chem. Rev. **95** (1995) 559–614. [*CrossRef*]

[105] X. Glipa et al., Solid State Ionics **97** (1997) 227–232. [*CrossRef*]

[106] T. Uma et al., Chem. Mater. **19** (2007) 3604–3610. [*CrossRef*]

[107] V.G. Ponomareva et al., Russ. J. Inorg. Chem. **51** (2006) 343–346. [*CrossRef*]

[108] C. Sun et al., Electrochim. Acta **53** (2008) 6417–6422. [*CrossRef*]

[109] C.D. Zangmeister et al., J. Solid State Chem. **180** (2007) 1826–1831. [*CrossRef*]

[110] E. Ortiz et al., J. Phys. Condens. Matter **18** (2006) 9561–9573. [*CrossRef*]

[111] C.R.I. Chisholm et al., Solid State Ionics **136–137** (2000) 229–241. [*CrossRef*]

[112] C.R.I. Chisholm et al., Acta Crystallogr. Sect. B Struct. Sci. **55** (1999) 937–946. [*CrossRef*]

[113] S.M. Haile et al., Solid State Ionics **77** (1995) 128–134. [*CrossRef*]

[114] B.V. Merinov et al., Phys. Chem. Chem. Phys. **23** (2021) 17026–17032. [*CrossRef*]

[115] W. Munch et al., Solid State Ionics **77** (1995) 10–14. [*CrossRef*]

[116] P. Zetterstrom et al., Solid State Ionics **116** (1999) 321–329. [*CrossRef*]

[117] N. Agmon et al., Chem. Phys. Lett. **244** (1995) 456–462. [*CrossRef*]

[118] S. Cukierman et al., Biochim. Biophys. Acta - Bioenerg. **1757** (2006) 876–885. [*CrossRef*]

[119] E.J. Murphy et al., J. Appl. Phys. **35** (1964) 2609–2614. [*CrossRef*]

[120] J.M. Pollock et al., J. Chem. Phys. **51** (1969) 3608–3614. [*CrossRef*]

[121] M. O'Keeffe et al., J. Phys. Chem. Solids **28** (1967) 211–218. [*CrossRef*]

[122] T. Dippel et al., Solid State Ionics **46** (1991) 3–9. [*CrossRef*]

[123] K.D. Kreuer et al., Berichte Der Bunsengesellschaft Fur Phys. Chemie **96** (1992) 1736–1742. [*CrossRef*]

[124] X. Guo et al., Int. J. Hydrogen Energy **38** (2013) 16387–16393. [*CrossRef*]

[125] Y. Matsuo et al., Solid State Commun. **130** (2004) 411–414. [*CrossRef*]

[126] T. Matsui et al., J. Power Sources **196** (2011) 9445–9450. [*CrossRef*]
[127] G.V. Lavrova et al., Solid State Ionics **179** (2008) 1170–1173. [*CrossRef*]
[128] P. Bocchetta et al., Electrochem. Commun. **6** (2004) 923–928. [*CrossRef*]
[129] G. Qing et al., J. Appl. Electrochem. **47** (2017) 803–814. [*CrossRef*]
[130] A.B. Papandrew et al., Chem. Mater. **23** (2011) 1659–1667. [*CrossRef*]
[131] D.K. Lim et al., Electrochim. Acta **288** (2018) 12–19. [*CrossRef*]
[132] D.C. Orozco et al., J. Power Sources **408** (2018) 7–16. [*CrossRef*]
[133] Y.K. Taninouchi et al., J. Mater. Chem. **17** (2007) 3182–3189. [*CrossRef*]
[134] A. Cholewinski et al., Polymers (Basel). **13** (2021) 1–20. [*CrossRef*]
[135] H. Elsayed et al., Ceram. Int. **46** (2020) 25299–25305. [*CrossRef*]
[136] F. Maglia et al., J. Mater. Res. **27** (2012) 1975–1981. [*CrossRef*]
[137] T. Xiao et al., Prog. Nat. Sci. Mater. Int. **30** (2020) 743–750. [*CrossRef*]
[138] I.M. Hung et al., J. Eur. Ceram. Soc. **35** (2015) 163–170. [*CrossRef*]
[139] T. Miyake et al., J. Phys. Condens. Matter **28** (2016) 23001. [*CrossRef*]
[140] R. Annapragada et al., Inorganica Chim. Acta **546** (2023) 121304. [*CrossRef*]
[141] B. Liu et al., Chem. Sci. **10** (2019) 556–563. [*CrossRef*]
[142] A. Gorre et al., J. Macromol. Sci. Part A Pure Appl. Chem. 60 (2022) 38–50.
[*CrossRef*]
[143] W. Zhou et al., Solid State Ionics **179** (2008) 380–384. [*CrossRef*]
[144] T.H.E. Lewis et al., Defin. ACIDS BASES **1810** (1943) 51–57.
[145] P. Gupta et al., Catal. Today **236** (2014) 153–170. [*CrossRef*]
[146] Y. Chen et al., Nat. Chem. **2** (2010) 503–508. [*CrossRef*]
[147] M.A. Hickner et al., Chem. Rev. **104** (2004) 4587–4611. [*CrossRef*]
[148] A.I. Baranov et al., J. Exp. Theor. Phys. Lett. **36** (1982) 459.
[149] Y. Yamane et al., Solid State Ionics **179** (2008) 483–488. [*CrossRef*]
[150] W. Zhou et al., Solid State Ionics **179** (2008) 380–384. [*CrossRef*]
[151] S. Hayashi et al., Solid State Ionics **171** (2004) 289–293. [*CrossRef*]
[152] Y. Li et al., Sci. Rep. **7** (2017) 1–10. [*CrossRef*]
[153] B. V. Tilak et al., Electroanal. Chem. Interfacial Electrochem. **48** (1973) 1–23.
[*CrossRef*]
[154] T. Uda et al., Electrochem. Solid-State Lett. **8** (2005) A245–A246. [*CrossRef*]
[155] A.S. Bondarenko et al., J. Power Sources **194** (2009) 843–846. [*CrossRef*]
[156] Z. Jiraak et al., Phys. Status Solidi **100** (1987) K117–K122. [*CrossRef*]
[157] D.A. Boysen et al., Science **303** (2004) 68–70. [*CrossRef*]